MESOSCALE AIR-SEA INTERACTION GROUP

TECHNICAL REPORT

DYNAMICS OF THE COUPLED ICE-OCEAN SYSTEM IN THE MARGINAL ICE ZONE: STUDY OF THE MESOSCALE PROCESSES AND OF CONSTITUTIVE EQUATIONS FOR SEA ICE

BY

SIRPA HAKKINEN

GEOPHYSICAL FLUID DYNAMICS INSTITUTE

FLORIDA STATE UNIVERSITY

TALLAHASSEE, FLORIDA 32306

DECEMBER 1984

NASA - MARGINAL ICE ZONE Grant NAG 5-219

and ONR Contract N00014-82-C-0404

MESOSCALE AIR-SEA INTERACTION GROUP

TECHNICAL REPORT

DYNAMICS OF THE COUPLED ICE-OCEAN SYSTEM IN THE MARGINAL ICE ZONE: STUDY OF THE MESOSCALE PROCESSES AND OF CONSTITUTIVE EQUATIONS FOR SEA ICE

BY

SIRPA HAKKINEN

GEOPHYSICAL FLUID DYNAMICS INSTITUTE

FLORIDA STATE UNIVERSITY

TALLAHASSEE, FLORIDA 32306

DECEMBER 1984

NASA - MARGINAL ICE ZONE Grant NAG 5-219

and ONR Contract N00014-82-C-0404

FOREWARD

This report is the Ph.D. dissertation of Ms. Sirpa Häkkinen. It is the latest contribution to modelling the ice and ocean in the Marginal Ice Zone. There are three major findings.

A new model for the constitutive equations is deduced from Reiner-Revlin theory. These equations are qualitatively more realistic than previously used constitutive relations.

The ice-ocean model is integrated in an x-y-t system with varying wind stress fields. A new mechanical mechanism for formation of ice banding is proposed. The physics of ice-edge upwelling is described in detail. It is shown that variations in ice concentration and/or ice edge configuration can generate oceanic eddies through differential Ekman pumping. It is hypothesized that oceanic eddies are formed by air-ice-sea interaction and not as hydrodynamic instability of ocean currents.

The ice-ocean model is very simple, but it is important to recognize that the horizontal scales in the marginal ice zone are very small. The grid spacing for ice-ocean models must be on the order of 0.5 - 1 km. for proper understanding of the ice dynamics. Ice models with grid spacings of 100 km. and larger cannot simulate any of the physics of the marginal ice zone.

The next task is to incorporate the thermodynamic model of Lars Petter Røed into this model and improve the vertical resolution of the ocean. In addition, we expect very interesting results will be found when we include actual land boundaries and a more comprehensive atmospheric boundary layer.

James J. O'Brien
Meteorology & Oceanography
The Florida State University

ABSTRACT

This study is aimed at the modelling of mesoscale processes such as up/downwelling and ice edge eddies in the marginal ice zones. A 2-dimensional coupled ice-ocean model is used for the study. The ice model is coupled to the reduced gravity ocean model (f-plane) through interfacial stresses. The constitutive equations of the sea ice are formulated on the basis of the Reiner-Rivlin theory. The internal ice stresses are important only at high ice concentrations (90-100%), otherwise the ice motion is essentially free drift, where the air-ice stress is balanced by the ice-water stress.

The model was tested by studying the upwelling dynamics. Winds parallel to the ice edge with the ice on the right produce upwelling because the air-ice momentum flux is much greater than air-ocean momentum flux, and thus the Ekman transport is bigger under the ice than in the open water.

The upwelling simulation was extended to include temporally varying forcing, which was chosen to vary sinusoidally with 4 day period. This forcing resembles successive cyclone passings. In the model with thin oceanic upper layer, ice bands were formed. The up/downwelling signals do not disappear in wind reversals because of nonlinear advection. This leads to convergences and divergences in oceanic and ice velocities which manifest themselves as ice banding. At least one wind reversal is needed to produce one ice band.

A constant wind field exerted on a varying ice cover will generate vorticity leading to enhanced up/downwelling regions, i.e., wind forced

vortices. Steepening and strengthening of the vortices are provided by the nonlinear terms. As in the case of ice band formation, the wind reversals will separate the vortices from the ice edge, so that the upwelling enhancements are pushed to the open ocean and the downwelling enhancements underneath the ice.

ACKNOWLEDGEMENTS

This work was supported by the National Aeronautics and Space Administration-Marginal Ice Zone No. 261338-506. NASA also provided the financial support to go on a research cruise to the Fram Strait in the summer of 1983. Partial support was obtained from the Office of Naval Research. The computations were performed at The Florida State University.

I would like to express my appreciation to Suomen Kulttuurirahasto (The Finnish Cultural Foundation) for their financial support during my studies in the United States.

I wish to express my gratitude and appreciation to Dr. James J. O'Brien for his support as my major professor. I wish to thank Dr. Lars Petter Roed as my co-major professor for the guidance and encouragement during this work. I am also grateful for the time taken by Drs. Georges Weatherly, Christopher Tam, Albert Barcilon and Allan Clarke while serving on my doctoral committee. Special thanks go to Dr. Benoit Cushman-Roisin for many useful discussions.

I would like to thank the Norwegian Polar Institute and especially Dr. Torgny Vinje for their hospitality during my Fram Strait cruise.

I am very appreciative to Helen McKelder for preparation and typing of my manuscript, James Merritt for his invaluable aid with the graphics and Dewey Rudd for drafting help.

TABLE OF CONTENTS

1. Introduction

The topic of this doctoral research is the dynamics of the marginal ice zone (MIZ). The study is aimed at the modelling of mesoscale processes such as upwelling and ice edge eddies. The modelling of the coupled ice-ocean system requires the construction of a constitutive law for sea ice.

The marginal ice zone can be defined to be that area connected to the edge of the pack ice where the existence of the ice edge has influence on the dynamics of the ice and the ocean (about 100-200 km inwards and outwards from the actual ice edge). In the northern hemisphere the MIZ regions are found in the Bering, Greenland and Barents Seas. The MIZs are areas of highly energetic interactions between the atmosphere, the ice and the ocean. They are characterized by mesoscale processes such as upwelling, oceanic fronts and eddies. The strong vertical and horizontal temperature gradients also lead to vigorous heat exchange between atmosphere and ocean. Moreover, there are considerable fluctuations in the position of the ice edge on time scales of a few days to years.

There is an increasing amount of observational evidence from the MIZ, and new experiments are planned currently. The MIZ has long been known by fishermen to be a biologically active area. It provides a congregation area for marine mammals and birds in

subpolar regions (Alexander, 1980). Interest in coastal upwelling which supports high primary production led various scientists to investigate upwelling and other related processes at the ice edge in the 1970's. Oil drilling and transportation in the polar seas has also increased the research efforts in the Arctic regions. The climatologists are interested in the MIZ because of the influence of the sea ice on the global climate. There are strong empirical correlations between interannual atmospheric variability and ice edge fluctuations. The MIZ provides a good opportunity for meteorologists to measure boundary layer modifications; for example, how the stability conditions and varying surface roughness affect the bulk aerodynamic coefficients (The Polar Group, 1980). In addition, the MIZ processes are important in defining the boundary conditions in large-scale ice models.

Upwelling at the ice edge is a well-documented phenomenon (Buckley et al., 1979; Alexander and Niebauer, 1981; Johannessen et al., 1983). The upwelling is described to be wind-generated and dynamically similar to coastal upwelling. The wind driven ice edge jet and its oceanic counterpart are observed during upwelling (Johannessen et al., 1983).

The ice edge is found to meander during calm periods (Johannessen et al., 1983; Nikolayev, 1973) and to shed eddies to the open water with scale of the Rossby radius of deformation. Also satellite imagery (Buckley et al., 1979, Vinje, 1977) has shown

that the ice edge can move tens of kilometers in a few days. There will be more discussion about observations in the MIZ in section 2.

The observational data from the MIZ's will considerably increase during the coming years when the Marginal Ice Zone Experiment (MIZEX) is carried out. Already during the 1970's when the Arctic Ice Dynamics Joint Experiment (AIDJEX) was taking place the U.S. National Academy of Sciences recommended a focusing of attention on the Arctic MIZ. The Joint Scientific Committee of the World Climate Research Program put forward in 1981 a recommendation for a comprehensive study of the MIZ physical processes.

MIZEX is a series of experiments, the first of which has already taken place in the Bering Sea MIZ mid-winter 1982-83. The summer experiment 1983 in the East Greenland MIZ was a pilot study for a larger experiment in the summer 1984 in this same area. Furthermore, there are plans for experiments in the Bering Sea in the winter 1984-85 and for a major East Greenland experiment in 1987.

Theoretical studies of the MIZ are very few. These have mostly concentrated on studying upwelling circulation. The possibility of the ice edge upwelling was first presented by Gammelsrod et al. (1975) using a one-dimensional, homogeneous model for the ocean. The ice cover was allowed to move vertically in the model. The discontinuity in wind stress (infinite stress curl) causes divergence in the oceanic velocities and hence upwelling at

the ice edge. At the steady state the ocean under the ice cover and outside the wind belt is quiescent. The upwelling occurs at the ice edge, and to satisfy the mass balance there is downwelling at the outer edge of the wind belt, and inside the belt there are off-ice and on-ice currents in the top and bottom frictional layers respectively.

With vertical stratification and a rigid lid in place of the ice cover, the analytical work by Clarke (1978) and the numerical model by Niebauer (1981) establish the scale of upwelling to be the Rossby radius of deformation and also the existence of the oceanic ice edge jet. The dynamical cause is again the infinite stress curl at the ice edge. Clarke (1978) also included the case of shelf ice edge upwelling (ice is thicker than the depth of the pycnocline) in which case the dynamics is governed by long wind-forced trapped waves travelling with the ice on the right (northern hemisphere).

In the above models the ice cover plays a passive dynamical role. However, the ice edge has been observed to move several times the Rossby radius of deformation in a few days, so its effect on upwelling dynamics can be significant. The internal ice stress is shown to have strong influence on the upper ocean dynamics when there are no other stresses present, Roed and O'Brien, 1981, 1983. Their model consists of coupled dynamical equations for the ice ice and for the ocean in one dimension, the ocean model is a reduced

gravity model. In the geostrophic adjustment process a strong ice edge jet will develop. The discontinuity at the ice edge in the surface stress generated by the moving ice causes an infinite divergence and upwelling, further under the ice there is downwelling because the decreasing ice velocity produces convergence of the water underneath. In the adjustment process the ice edge will move up to 20 km or more depending on the parameterization of the internal ice stress from its original position.

The effect of the moving ice can change the upwelling found in the rigid-lid cases into downwelling (Roed and O'Brien, 1983). Also the bulk aerodynamic coefficients or actually their relative magnitude are of significant importance in determining whether the ocean response to winds is upwelling or downwelling (Roed, 1983).

In this paper, the model of Roed and O'Brien is extended to two dimensions to study baroclinic motion as a response to local forcing, i.e., upwelling, and how different variations in the ice field, like a meandering ice edge and varying ice concentration (with a straight ice edge), lead to eddy-motion in the ocean. The study of barotropic instability processes in the MIZ is also included. All these processes may produce meandering of the ice edge and mesoscale oceanic eddies. There have been no modelling efforts addressing these subjects. The formulation of the numerical model is given in Section 3.1.

For a dynamical model of the ice the internal ice stresses need to be specified, which is the other main topic of this study. In the literature three different rheologies have been associated to the ice medium: viscous (Doronin, 1970; Campbell, 1965), elastic-plastic (or rigid plastic) (AIDJEX-modellers, Pritchard, 1975, 1980; Coon, 1974, 1981; Coon, et al., 1974; Colony and Pritchard, 1975); Pritchard and Reimer, 1978) and viscous-plastic (Hibler, 1977). Although plastic constitutive laws are widely used in large-scale ice modelling, they have not been established experimentally. In Section 3.2 a constitutive law for the ice is proposed. It is based on Reiner-Rivlin theory of generalized viscous fluids, in which the viscosity coefficients depend on the strain-rate invariants and some other relevant external parameters, like ice concentration and thickness.

The hydrographic sections for summertime and early fall indicate that pycnocline changes are comparable to the upper layer thickness. This makes the dynamics strongly nonlinear. The scaling of the dynamical equations and major balances are discussed in Section 3.3.

A review on upwelling dynamics and stability analysis are given in Sections 4.1 and 4.2 with the inclusion of the nonlinear (thin upper layer) case. In section 4.3 a new theory for ice band formation is given. When a constant wind field is changed to a temporally varying field, there will be generation of ice bands.

The time-varying winds simulate cyclone passings. It is shown in Section 4.3 that nonlinear dynamics is essential for the formation of ice bands.

Section 5 deals with the effect the different kinds of disturbances in the ice field induce on the ocean when forced by local winds. The ice cover variation along the ice edge will lead to differential Ekman pumping and produce eddy like features that travel with the speed of the ice. These up-(down-)welling enhancements are not unstable and they do not separate themselves from the ice disturbance that supports their existence. The cyclonic eddies can be shed to the open ocean in wind reversal due to nonlinear advection.

2. Observations in the MIZ

The MIZ of the northern hemisphere lies in the East Greenland Sea which is of great importance for general circulation as an area for the Arctic Bottom Water formation. In the Greenland Sea the Atlantic waters and Polar waters are recirculating. The Atlantic water enters to the Greenland-Iceland basin as an extension of the Norwegian Atlantic Current which separates to a part that continues to the north along the western side of Spitsbergen and to a part that flows to the Barents Sea (Swift and Aagaard, 1981). The mass transports are of order 7 Sv (Coachman and Aagaard, 1974). The Barents Sea branch joins the recirculation gyre north of Spitsbergen, where the flow follows the ice edge towards the south. Smaller amounts of the Atlantic water enters through the Denmark strait (the northward branch of the Irminger Current). The cold and less saline Polar waters flow southward along the western side of the basin forming the East Greenland Current.

The Atlantic water suffers a tremendous heat loss during wintertime off the coast of Spitsbergen. The maximum heat flux is nearly twice the maximum of the Gulf Stream (which occurs north-east of Cape Hatteras) (Gorshkov, 1983). This water flows south adjacent to the East Greenland Current forming the Polar front. The Polar front and the coldest water, -1.4°C at 1000 m,

are found off the East Greenland shelf break (Swift and Aagaard, 1981), where also the wintertime marginal ice zone is located.

Upwelling in the MIZ has been confirmed by observations (Buckley et al. (1979) north of Spitsbergen, Alexander and Niebauer (1981) in the Bering Sea and Johannessen et al. (1983), north of Spitsbergen. The hydrographic sections show frontal structure, one front at the ice edge and another one further out (10-60 km) from the ice edge. The fronts are more pronounced in the melting period (Alexander and Niebauer, 1981). This structure can be explained by upwelling generated by wind, although Alexander and Niebauer could explain only 1/10 to 1/2 of the area of upwelled water by wind-driven Ekman transport for some of their hydrographic sections. In the presence of strong easterly winds (15 m/s), the pycnocline is lifted 5 to 7 meters (Johannessen et al., 1983). The data of Buckley et al. (1979) shows upwelling even with very weak winds. The width of the upwelled area is observed to be 2-3 times the Rossby radius of deformation. This fact can be related to the ability of the ice edge to move tens of kilometers in a few days. This is confirmed by satellite imagery (Vinje, 1977).

An oceanic ice edge jet (speed of order 10 to 20 cm/s) is observed and attributed to be wind driven similar to the jet in the ice with a speed of about 30 cm/s at 5 km from the edge, Johannessen et al., 1983. They calculated the drift factors (percentage

of the wind velocity) for the ice in the interior and at 50 km from the edge to be 0.9% and 1.2% respectively, while at the edge the value of 1.9% was established. Nikolayev (1973) found a surface jet at the ice edge (in the Chuckhi Sea) which traveled with the open water on the right independently of the wind direction. The existence of these strong oceanic and ice jets implies strong horizontal and vertical shears which in turn can cause barotropic and baroclinic instabilities.

Johannessen et al. (1983) has reported that the ice edge and the ice-edge front meanders with a scale of 20-40 km. The meandering happened during calm periods. On the other hand, with winds parallel to the ice edge, the ice edge appeared to be straight. Nikolayev (1973) observed meandering of the ice-edge front current in the Chuckhi Sea in aerial surveys, but with larger wavelength (about 100 km). Oceanic mesoscale eddies are often seen at the MIZ in satellite imagery (Vinje, 1977; Wadhams, 1981). The eddies obviously are closely connected to the existence of the ice edge, and they usually have been attached to the edge. Moreover, they are often marked by grease ice, which is used to identify eddies in satellite pictures. The dimensions of these eddies are 10-20 km which is of the order of the Rossby radius of deformation. Hydro-graphic data confirms the existence of eddies of the same scale and that these features are confined to the mixed layer. The observed eddies have been cyclonic (Johannessen et al., 1983).

Due to lack of good observational data there is no information on the growth-rates and lifetimes of these eddies. There is some evidence that the smaller eddies live at least 8 to 10 days (the time buoys have been able to track them) (Johannessen et al., 1983).

While eddies of scales 10-20 km are the most abundant, there has been observations of a 60-90 km eddy in the Greenland Sea lying over the Molloy Deep (79° 40'N, 3°E) (Wadhams, 1983) and 100-200 km eddies have been seen in satellite pictures from the Bering Sea. The former eddy, which is frequently seen in satellite pictures, can not be explained as resulting from an instability process because it is very stagnant and shows no downstream propagation.

There is a persistent phenomenon of regularly spaced bands of ice floes especially in the Bering Sea MIZ with scales of order 1-10 km. These bands appear when winds are off-ice, with their long axes oriented nearly normal to the wind direction. The bands have not been seen when winds are blowing towards the ice (Bauer and Martin, 1980; Muench and Charnell, 1977). Speeds of 20-30 cm/s are considered typical translation speeds for the ice bands, Muench et al. (1983). They believe that bands result from interaction with internal gravity waves. Other explanations have also been offered (Wadhams, 1983; McPhee, 1982).

3. The Coupled Ice-Ocean Model

3.1 The Model Formulation

For the study of the wind forced motion in the coupled ice-ocean system a 2-dimensional numerical model was constructed. The model is in a Cartesian coordinate system rotating with a uniform angular velocity f/2. The Coriolis parameter f was chosen to be that of the latitude 80° ($f = 1.4 \cdot 10^{-4}$).

The sea ice model consisting of the two momentum equations and the equation for the continuity of the ice concentration is coupled to a reduced gravity ocean model through interfacial stess. The external forcing is applied through stresses at the air/ice and air/ocean interfaces. The air/ice stress is proportional to the ice concentration (=compactness) and the air/ocean stress to the fraction of the area free of ice.

If there is a spatially varying ice thickness, one more equation is needed to solve the dynamical system. A convenient solution is to select the continuity equation both for the total mass and for the ice concentration. Then the ice thickness is available through a simple division. Compared to the large scale sea ice models (Hibler (1979), Hibler and Tucker (1979), Hibler and Walsh (1982)), there are no redistribution terms in the continuity

equations, i.e. the equation of state is dD/dt = 0, and the thickness, D, is conserved along the particle path. The so called sea surface tilt terms are not included in this ice model.

The transport form was chosen for the oceanic model to make the continuity equation linear, i.e. U=hu and V=vh, where u and v are the x-and y-velocity components respectively and h is the upper layer thickness. The governing equations of the problem are the following:

for the ice

$$\rho_i AD\,(u_{i,t}+u_i u_{i,x}+v_i u_{i,y}) = \rho_i AD f v_i + A(\tau_{ai,x} + \tau_{wi,x}) + F_{i,x} \tag{3.1.1}$$

$$\rho_i AD\,(v_{i,t}+u_i v_{i,x}+v_i v_{i,y}) = -\rho_i AD f u_i + A(\tau_{ai,y} + \tau_{wi,y}) + F_{i,y} \tag{3.1.2}$$

$$A_t + (Au_i)_x + (Av_i)_y = 0 \qquad (0 \leq A \leq 1) \tag{3.1.3}$$

$$m_t + (mu_i)_x + (mv_i)_y = 0, \qquad m = \rho_i AD \tag{3.1.4}$$

and for the ocean

$$U_t+(U^2/h)_x+(UV/h)_y = fV - \frac{g^*}{2}\frac{\partial h^2}{\partial x} + ((1-A)\tau_{aw,x} - A\tau_{wi,x})/\rho + A_H\nabla^2 U \tag{3.1.5}$$

$$V_t+(UV/h)_x+(V^2/h)_y = -fU - \frac{g^*}{2}\frac{\partial h^2}{\partial y} + ((1-A)\tau_{aw,y} - A\tau_{wi,y})/\rho + A_H\nabla^2 V \tag{3.1.6}$$

$$h_t + U_x + V_y = 0 \tag{3.1.7}$$

where $F_{i,x} = \frac{\partial \sigma_{xx}}{\partial x} + \frac{\partial \sigma_{xy}}{\partial y}$, $F_{i,y} = \frac{\partial \sigma_{yy}}{\partial y} + \frac{\partial \sigma_{xy}}{\partial x}$ are the forces due to the internal ice stress, σ is the stress tensor for ice,

$\underset{\sim}{\tau}_{ai}$ is the stress exerted by air on ice with components $\tau_{ai,x}$, $\tau_{ai,y}$,

$\underset{\sim}{\tau}_{wi}$ is the water-ice stress with components $\tau_{wi,x}$, $\tau_{wi,y}$,

$\underset{\sim}{\tau}_{aw}$ is the air-water stress with components $\tau_{aw,x}$, $\tau_{aw,y}$,

A is the ice compactness (varies between 0 and 1),

D is the ice thickness,

ρ_i, ρ and ρ_a are the ice, water and air densities (ρ_i = 910 kgm^{-3}),

g^* is the reduced gravity,

and A_H is the horizontal eddy viscosity coefficient.

There is a weak Laplacian diffusion term in both of the continuity equations for sea ice. They are needed to damp out the possible nonlinear instabilities. As it can be seen from (3.1.3) and (3.1.4), A (m) can vary from 1 ($\rho_i D$) to 0, which would correspond to surfacing of the pycnocline in an ocean model.

The lateral stresses are parameterized using quadratic forms:

air/ice stress $\underset{\sim}{\tau}_{ai} = \rho_a C_{ai} |\underline{W}_a - \underline{U}_i| (\underline{W}_a - \underline{U}_i) = \rho_a C_{ai} |\underline{W}_a| \underline{W}_a$

air/water stress $\underset{\sim}{\tau}_{aw} = \rho_a C_{aw} |\underline{W}_a| \underline{W}_a$

ice/water stress $\underset{\sim}{\tau}_{iw} = \rho_i C_{iw} |\underline{U}_i - \underline{U}_w| (\underline{U}_i - \underline{U}_w)$

where $\underline{W}_a$, $\underline{U}_i$ and $\underline{U}_w$ are the wind, ice and water velocity vectors respectively. The drag coefficient at the air/ice interface (C_{ai})

depends on ice concentration, how rough the ice is, etc., but in general C_{ai} is 2 to 3 times the drag coefficient over the open water (C_{aw}). In very unstable conditions C_{aw} can be larger than C_{ai} (Macklin (1983); Walter et al. (1984)). In this study C_{ai} and C_{aw} are taken to be 3.6×10^{-3} and 1.2×10^{-3} respectively.

There is a great variety of studies on the interfacial ice/water stress showing that the coupling is strong (Pease et al. (1983), McPhee (1982)). The stress depends on how smooth or rough the bottoms of the ice floes are, the and multiyear ice which is heavily ridged is bound to lead to a different parametrization than smooth one year ice. In the following computations C_{iw} is fixed to be $10 \cdot 10^{-3}$ or $15 \cdot 10^{-3}$ which are in accordance with the measurements of Pease et al. (1983) but are larger than the value of $5.5 \cdot 10^{-3}$ used by Hibler (1979). If the ice-water drag coefficient is large, then the variation in ice thickness does not greatly affect the ice velocities. For small drag the Coriolis force becomes more important allowing the thickness of the ice to have a larger effect on the ice velocity.

In the Arctic the baroclinic radius of deformation is very small compared to the values at the midlatitudes. The σ_t profile in figure (1) using vertical normal mode separation yields 4.24 km (for depth of 500 m) to 5.43 km (for depth of 2000 m) for the deformation radius of the first baroclinic mode. Because the ocean is simulated with a two-layer model, where the lower layer is infinitely deep and

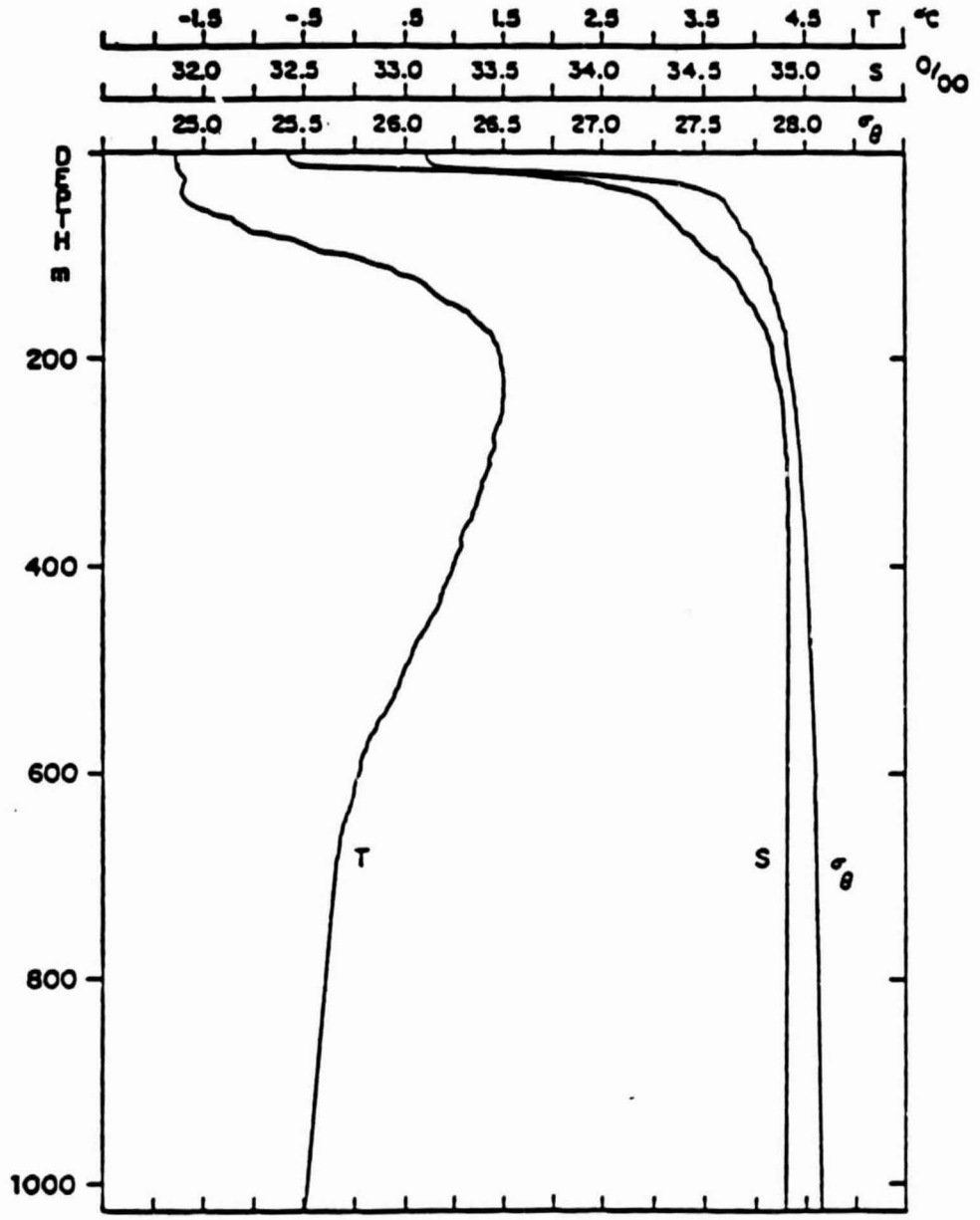

Figure 1. The temperature, salinity and density structure in the Greenland Sea in early Fall 1979. From Johannessen et al. (1980).

at rest (the reduced gravity model), the $g^* = g(\rho_2 - \rho_1)/\rho_2$ and the upper layer thickness h are chosen so that it approximates the deformation radius in the above limits. In the following the values $g^* = .0172\ ms^{-2}$ and $h = 25$ m are used which correspond to $R_d = 4.68$ km ($f = 1.4 \cdot 10^{-4} s^{-1}$). These numbers correspond well to the summertime and early fall conditions in the Greenland Sea. In wintertime the upper layer thickness is 150-200 meters, which together with a density difference of 2.0 σ_t-units gives $R_d \sim 10$ km (figure 2).

The Numerical Model

The model consists of a channel 100 km long (x-direction) and 70 km wide (y-direction) (the size was chosen according to the maximum computer storage). One half of the channel is initially covered by ice, the other half is open water. This geometry will resemble the MIZ in the northern Greenland Sea, where the ice edge is found more or less in the north-south direction over the deep Greenland basin.

The dynamical equations are discretized on a staggered grid, which is shown in figure (3). The grid size was taken to be 1 km. Considering the resolution of the dynamics this value might be slightly too large, since there are 4-5 grid points per R_d.

Boundary Conditions

In their one-dimensional model Roed and O'Brien (1983) were able to solve for the ice edge position exactly using the method of

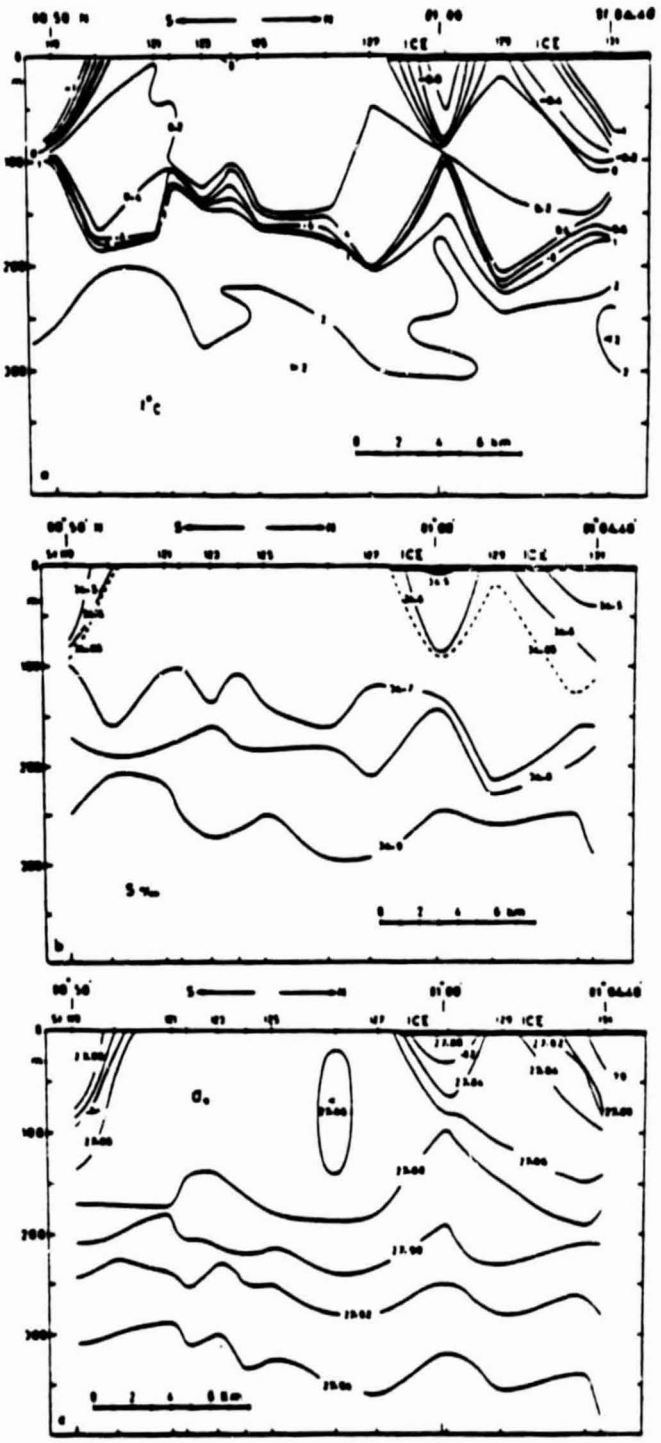

Figure 2. The hydrographic sections in the Greenland Sea marginal ice zone in December 1977. From Buckley et al. (1979).

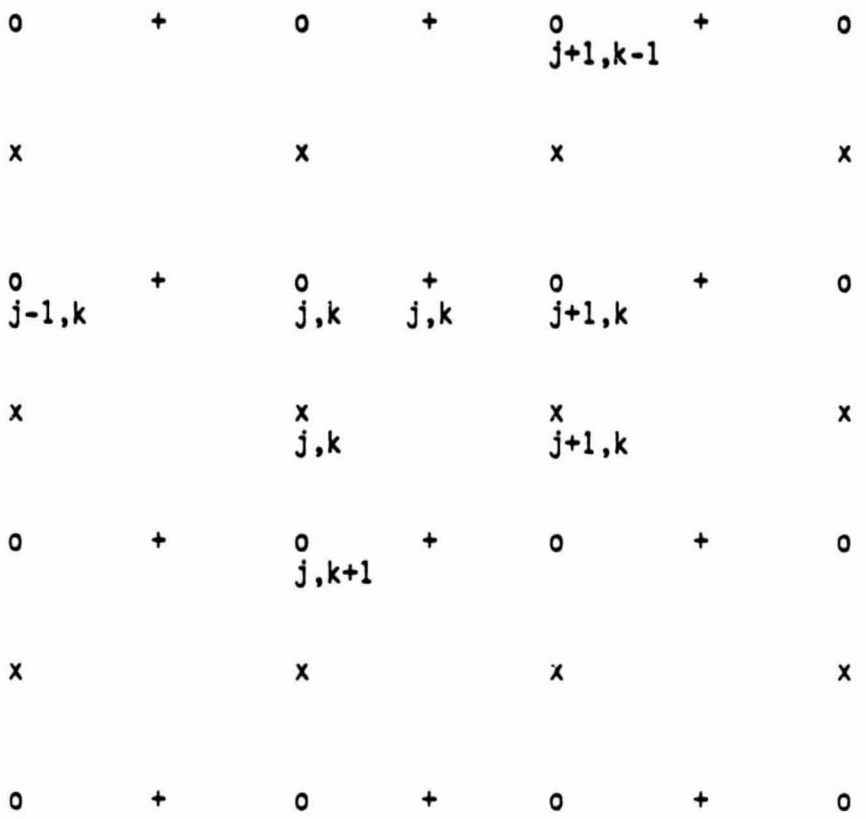

Figure 3. The staggered grid for the numerical model.
A and h are computed at o - points,
u_i and u are computed at + - points and
v_i and v are computed at x - points.

characteristics. This was possible because they had no viscous terms in the momentum equations. In two-dimensions the method of characteristics would be extremely tedious, and because of the viscous, terms very difficult. The incapability of solving for the exact ice edge position can be justified. If 8-10 grid points are needed to resolve the dynamics properly, then knowing the ice edge position better than one grid point cannot have any effect on the dynamics. In this model the ice edge is allowed to diffuse freely; the error that arises is not serious if the grid size is small (which is the case in this model). Also, the dynamics will depend more on the gradients in the ice concentration (or mass) than on the magnitude of the concentration.

When ice is moving to grid points where there was no ice before, the boundary condition for ice velocities at the ice edge is based on the continuity of stresses. This means that the ice stresses are equal to the water stresses, and because the viscosity of the water is negligible compared to the viscosity of ice, the stresses for the ice are approximated by $\sigma_{xx}(= u_{i,x}) = \sigma_{xy} = (u_{i,x}) = 0$ and $\sigma_{yy}\ (= v_{i,y}) = 0 = \sigma_{yx}\ (= u_{i,y})$ on the boundaries parallel to the y axis and to the x axis respectively.

On the north and south ends of the channel cyclic boundary conditions are applied. On the boundaries to the east and west open boundary conditions are used according to the formulations by Camerlengo and O'Brien (1980).

3.2 Constitutive Law for the Ice

3.2.1 Review of Earlier Stress Laws

A major physical assumption invoked in sea-ice modelling is to regard the pack ice field as a continuum. In the MIZ where the dynamical scale is the Rossby radius of deformation (about 5-10 km), this hypothesis can be well justified because the ice floe size is small. The diameter of the floes varies from 0.5 m up to 25 m in the first 10 km and from 25 to 50 m in the next 10-15 km and from 25 km inwards the maximum floe size is several hundred meters (Johannessen et al., 1983). The internal ice stress arises from the bumping and shearing between the individual ice floes comprising the ice medium. Although it has been recognized for some time that ice is a non-Newtonian fluid, a viscous law was used in the earliest large scale ice modelling attempts by Campbell (1965) and Doronin (1970). Glen has proposed a viscous law (1958, 1970) that has been used in large-scale ice models by Hibler and Tucker (1979).

The AIDJEX modellers adopted a view to treat ice as an elastic plastic medium. Plastic rheology has been preferred for the pack ice because observations show that the ice field can support varying strain rate states under fairly uniform forcing. In plasticity theory a condition for plastic yielding is introduced through the so called yield curve which is a function of stress invariants (or

principal stresses). Interior to the yield curve the stress is assumed to be elastic (or viscous (Hibler, 1977)), and points along the curve represent plastic yielding under constant stress. The yield curve can take a shape of a teardrop (AIDJEX modellers) or an ellipse (Hibler, 1977) which is confined to the negative principal stresses quandrant because of the inability of the ice to support tension.

Introducing an associated flow rule the plastic potential is assumed to be the same the yield curve and the strain rate, $\dot{\varepsilon}_{ij}$, can be computed from $\dot{\varepsilon}_{ij} = \lambda \, \partial\phi / \partial\sigma_{ij}$ where ϕ is the yield curve $\phi(\sigma_1, \sigma_2, p^*) = 0$, and p^* is the plastic strength, σ_1 and σ_2 are the principal stresses, σ_{ij} is a component of the stress tensor. The flow rule implies that the plastic flow is orthogonal to the yield curve. The plastic hardening may be taken into account by increasing the plastic strength.

Hibler (1977) used an elliptic yield curve to show that locally plastic law can stochastically give a viscous behavior of the ice in time scales of one day. In his stress law the effective shear and bulk viscosities will decrease for converging ice fields (although he has a lower bound for the viscosities). This means that with increasing convergence the stress stays the same (plasticity assumption). Contrary to this, one would expect the viscosities to increase with stronger convergence, e.g. preventing ridges to become infinitely high. These drawbacks of the plastic stress laws were

first pointed by out by Smith (1983). Hibler has a pressure term to smooth out excessive ridging, but it is difficult to interpret the physical meaning of this equilibrium pressure in large scale behavior of sea ice.

There are several arguments against plastic formulation and especially against the flow rule, which is introduced merely for mathematical convenience (Hunter, 1976). The extra assumption that the yield curve and the plastic potential (which was originally used in the flow rule) are the same is not necessarily true. There is no experimental evidence for any of the assumed yield conditions. There is also a controversy about the magnitude of the plastic strength. The large-scale ice models need a strength of 10^5 Nm^{-1} to be able to produce motion similar to observed (Pritchard, 1981; Hibler and Walsh, 1982) while the best theoretical value is an order of magnitude less (Rothrock, 1975, 1979).

3.2.2 The formulation of the constitutive law

There are two alternative approaches in postulating the constitutive law: 1) to assume that the stress depends only on the strain or the strain rate at that point and at that time, or 2) to assume that stress depends on the whole time history of the strain at a point (Astarita and Marrucci, 1974). Obviously the last approach would lead to a very complicated formulation. For

modelling purposes the most favorable description is the first one, which will be used in this study.

The general physical properties which are included in order to develop a constitutive law are

a) ice cannot support tension -- opening occurs with nearly no stress (no isotropic stress for diverging ice).

b) no equilibrium pressure -- ice does not have a tendency to expand by itself, i.e. no motion implies no stress.

c) the "memory effects" will come through the mass distribution or the so called compactness; with high compactness ice will resist more compression and shearing than for low compactness. It is approximated that with 85% ice coverage in the MIZ the floe interaction is already negligible. Also thick ice can resist more to deformation than thin ice.

d) the higher the compression (convergence) is, the more the ice will resist it. Observations indicate ridges are never higher than about 15 m. This implies that viscosity must become nearly infinite to stop ridging in converging ice fields: effective viscosity increases with compression.

e) high shear rates should give low effective viscosity to explain openings in coastal shear zones.

f) mathematical requirements: frame-indifference and dimensional invariance. The former states that the

constitutive law must be invariant under a change of coordinate system (also for anisotropic materials). This is also called 'principle of material objectivity' (a change of observer must leave the behavior of the material unaffected) implying isotropy in space. Dimensional invariance requires that there must be a minimum number of dimensional parameters including at least one with dimensions of stress, one with time and one with length.

g) the constitutive law must lead to positive dissipation.

A rigorous way to proceed in finding the constitutive law for the ice is the generalized Newtonian fluid theory although this prescribes 'viscosity' functions to be determined empirically. Reiner (1945) and Rivlin (1948, 1955) showed that if the stress is assumed to be a function of strain rate at that point and at that time then the stress can be expressed as $\underset{\sim}{\sigma} = \phi_0 \underset{\sim}{1} + \phi_1 \dot{\underset{\sim}{\varepsilon}} + \phi_2 \dot{\underset{\sim}{\varepsilon}}^2$ where ϕ_0, ϕ_1 and ϕ_2 are functions of the three strain rate invariants only. In two dimensions the third term is dropped, because the second and the third invariants coincide (Appendix). The above form is the only one that will satisfy the requirement of material objectivity. Furthermore the quantities ϕ_0, ϕ_1, (and ϕ_2) are material functions. By assigning these, the particular Reiner-Rivlin fluid is identified.

In the light of the above considerations, the constitutive law

of the ice can be written as

$$\sigma_{ij} = \phi_0(tr\dot{\underset{\sim}{\varepsilon}}, det\dot{\underset{\sim}{\varepsilon}}, S_p)\delta_{ij} + \phi_1(tr\dot{\underset{\sim}{\varepsilon}}, det\ \dot{\underset{\sim}{\varepsilon}}, S_p)\dot{\varepsilon}_{ij}, \quad (3.2.1)$$

(with i = 1,2 and j = 1,2) where S_p can be other scalar state variables like ice thickness, compactness, etc. The stress may be divided into isotropic and deviatoric parts:

$$\sigma_{ij} = (\phi_0 + \phi_1 tr\dot{\underset{\sim}{\varepsilon}}/2)\delta_{ij} + \phi_1\dot{\varepsilon}'_{ij} = \hat{\phi}_0\delta_{ij} + \phi_1\dot{\varepsilon}'_{ij} \quad (3.2.2)$$

where $\hat{\phi}_0$ may be called the 'pressure' and ϕ_1 the 'shear viscosity'. $\hat{\phi}_0$ and ϕ_1 can now be assigned so that they include the following properties:

- $\hat{\phi}_0$ is zero when there is no motion
- $\hat{\phi}_0 < 0$, only compressive isotropic stress will be allowed because ice has no resistance to tension and hence $\hat{\phi}_0$ should be zero for diverging ice ($\dot{\varepsilon}_{11} + \dot{\varepsilon}_{22} > 0$). We allow shearing ($\phi_1 \neq 0$) for high compactness even though the ice is diverging.
- $\hat{\phi}_0$, ϕ_1 depend on ice compactness (and ice thickness in large scales), high compactness should give high viscosity: In the MIZ 85% ice coverage (corresponds to A = .85) should give zero effective viscosity. The floes are then sufficiently separated so that they do not interact. If the ice coverage is 100% (the compactness reaches its maximum A = 1) and if the ice cannot ridge

(ice is confined to horizontal planes) the viscosity should go to infinity to prevent any further compression.

- For high shear rates the shear viscosity should be low. It has been observed that highest shears occur near shores where openings of the ice field also occur. As noted by Rothrock (1979) that in order for the viscous models to simulate the ice motion, the viscosity should vary from about $5 \cdot 10^9$ kg s^{-1} near shore to over 10^{11} kg s^{-1} far from shore. In Reiner-Rivlin theory this feature can naturally be taken into account.
- Generally shearing stresses are expected to be smaller than isotropic stresses because ice field resists compression more than shearing.

We hypothesize that the following formulae are a reasonable constitutive law and takes into account the assumptions listed above:

shear viscosity, $\phi_1 = \rho_i AD\mu_1 \exp(-\kappa(1-A))\exp(-\gamma\theta_1|\theta_2|)$ and

isotropic stress, $\hat{\phi}_0 = -\rho_i AD\mu_0 \exp(-\kappa(1-A)), \quad \theta_1 < 0.$

This law introduces four parameters to be fixed either from observations or from model experiments. The A-dependent part was chosen to have the same form as Hibler (1977) with $\kappa = 15$, giving a rapid decrease of the stress with decreasing ice concentration. The coefficient μ_0 was chosen to be 1 Nm/kg giving ice strength of order 10^3 Nm^{-2}. The shear coefficient, μ_1, was fixed to be 10^4 m^2/s, which corresponds to order of 10^7 kg/s in the units preferred by large

scale ice modellers. This value is nearly three orders of magnitude smaller than values extrapolated from observed ice motion (Rothrock (1979)) or used by ice modellers like e.g. Hibler (1979). The viscosities given in literature apply to large scale ice dynamics, scales of 200 to 500 km, but studying smaller scales one is able to resolve better the motion and the nonlinear advection that also contributes to the large scale viscosity. This means that there is a definite scale effect in the ice shear viscosity and it should rather be called the "eddy" viscosity of the ice.

The justification for the chosen value of μ_l can be based on the theory of turbulence (2-dim). The dissipation rate, ε, can be derived from the momentum equations and it is

$$\varepsilon = \mu |D|^2,$$

where D is deformation rate. Based on this equation we derive an equation for viscosity, μ, using dimensional analysis and assuming that μ depends only on ε and wavenumber, k:

$$\mu = C\ \varepsilon^{1/3} k^{-4/3} \qquad \text{(C is constant).}$$

The (turbulent) dissipation rate of the system is the same whether studying its behavior in large or small scales (scales designated by L_ℓ and L_s respectively), which leads to the following scale relation (appropriate wavenumber is inverse of length scale):

$$\mu_s = \mu_\ell (L_s/L_\ell)^{4/3}.$$

When L_s = 1 km, L_ℓ = 200 km, $\mu_\ell = (1\text{-}10)10^{10}$ kg/s (e.g. from

Rothrock, 1979), the small scale viscosity is $\mu_s = (1\text{-}10)10^7$kg/s, which is the value range used in this study.

The factor $e^{-\gamma\theta_1|\theta_2|}$ is added to account for the decrease of viscosity for high shear rates. The multiplication by the trace of strain rate tensor is needed because under compression it is harder to have shearing in the system. This is especially important near land boundaries. The coefficient γ was chosen to be $3 \cdot 10^8$ s^2. For typical values of θ_1 and θ_2, $(1\text{-}2)10^{-5}$ s^{-1} this factor is still 0.9 (for diverging ice). This comes into play only for very large shear and compression/tension rates.

The testing of the above constitutive law was done by studying the response of the ice to on-ice winds when the ice is bounded by a wall. The results for the two cases $\mu_0 = 0$ and $\mu_0 = 1.0$ Nm/kg are shown in figure (4) after three days of an on-ice wind of m/s. The initial ice concentrations are shown as dashed lines, the ice edge being at x=100.5 km and the solid boundary at x = 0. As seen from figure 4c the thickness of the ice can grow up to 34 meters if there is no resistance to compression during a wind event. When the isotropic stress is added, the maximum height that ice can pile up against the shore is 13 meters in three days (figure 4d). The distance from the boundary where the thickness changes take place are very different in these two cases. This is reflected also in the velocity profiles for the ice (figure 5). For the case $\mu_0 = 0$ the width of this boundary layer, δ, is determined by the viscosity

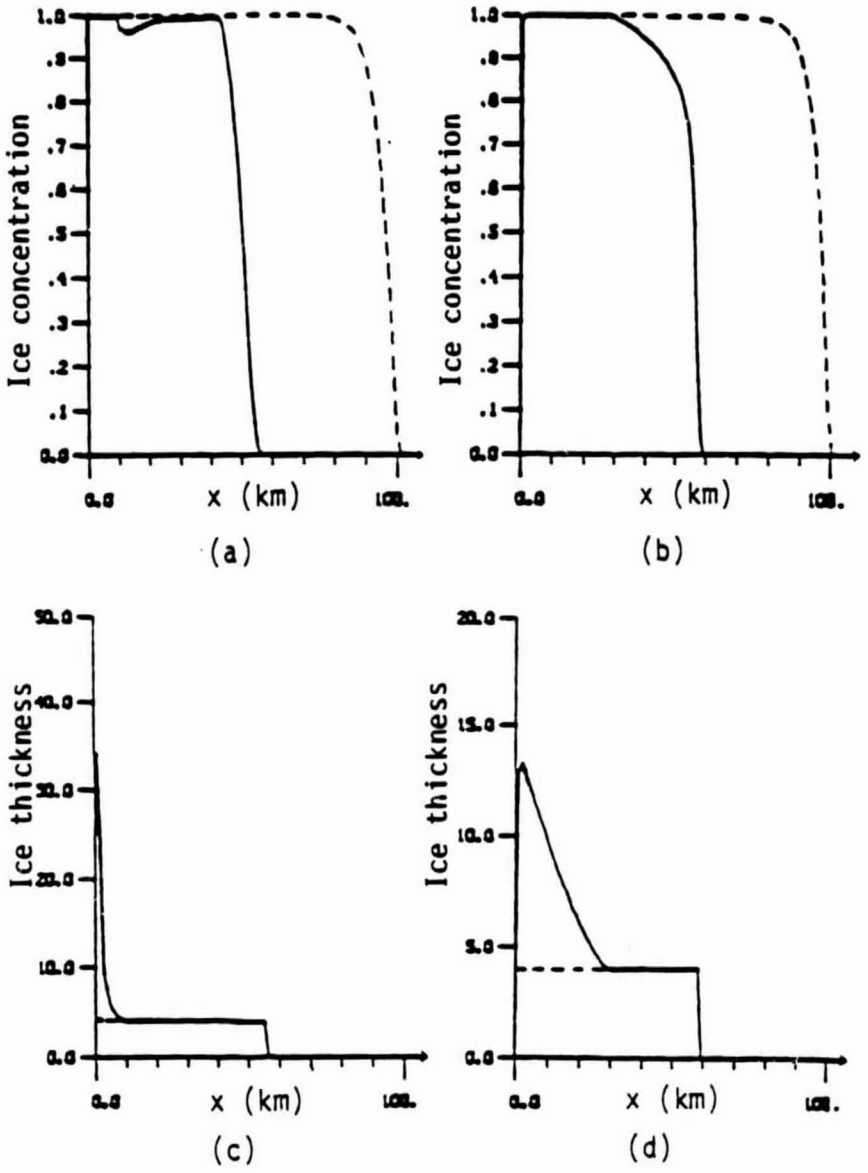

Figure 4. The ice concentrations (a), (b), and the ice thicknesses (c), (d), after 3 days of 10 m/s onshore wind. The land boundary is at x = 0. The initial values are shown with dashed lines. In (a) and (c) there is no isotropic stress, i.e. $\mu_o = 0$ and in (b) and (d) $\mu_o \neq 0$.

(Ekman-type side-wall boundary layer)

$$\delta = \sqrt{2\mu_1/f\rho} = 10 \text{ km.}$$

In the other case, $\mu \neq 0$, ice behaves like an ordinary barotropic fluid pushed towards the coast because of the existence of the isotropic stress. The ice thickness at the coast has its maximum when the pressure gradient, which is proportional to the ice thickness gradient, is balanced by the wind stress. At this steady state the thickness gradient is established across the whole ice extent.

Comparing the velocity profiles for $\mu_0 = 0$ and $\mu_0 = 1$ Nm/kg cases (figure 5), one sees that in the latter case (figure 5b), the velocities are overall smaller than in the $\mu_0 = 0$ case (figure 5a). This, is of course, due to the isotropic stress resisting the ice motion. Only near the ice edge where ice concentration is small (the internal ice stress is small) the ice velocities increase near to their free drift values. The ice edge velocity in figure (5a) is smaller than in figure (5b), because in the former the ice edge is steeper leading to larger viscosity (and smoothing). The v-velocity components of the ice are induced by the oceanic Ekman transport due to the strong interfacial stress. The cryospheric Ekman transport is negligible because the Coriolis term is small compared to other terms in the momentum balance for the ice.

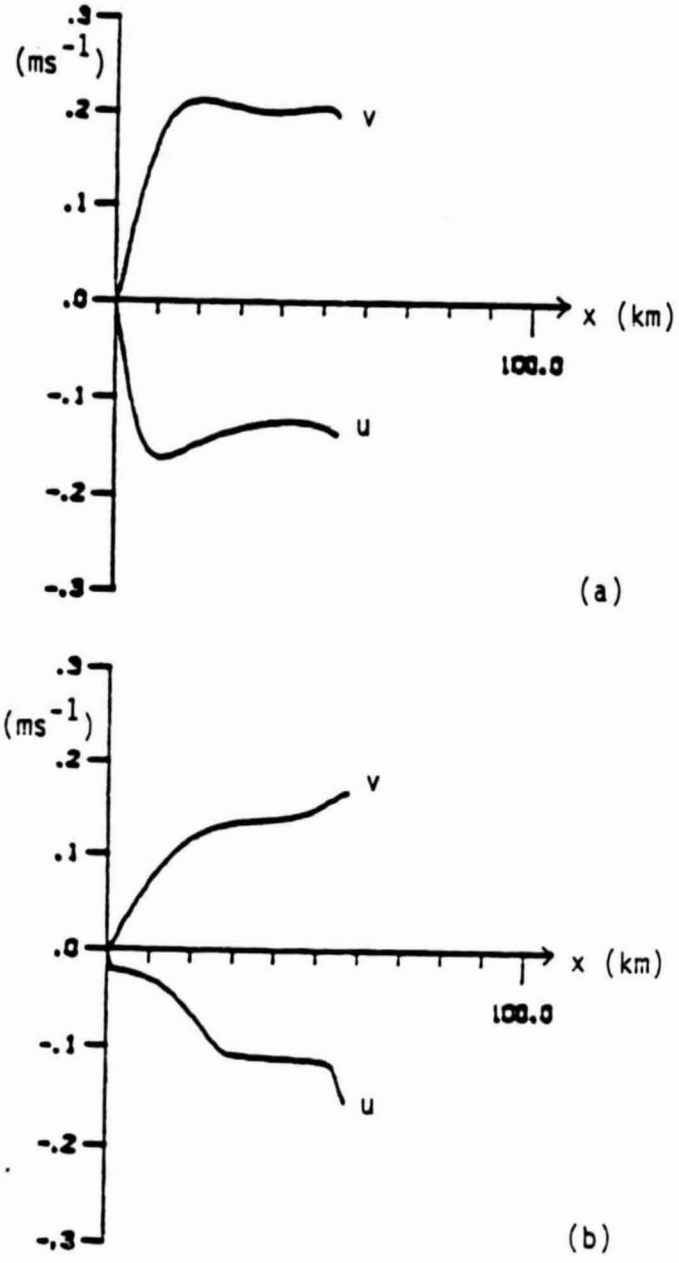

Figure 5. The u- and v-components of the ice velocity at day 3. In (a) $\mu_o = 0$, and in (b) $\mu_o \neq 0$.

The above simulation is not very realistic if one considers the Arctic ice pack in the wintertime, when the ice floes are frozen to each other forming an "ice plate", especially near coasts. One way of extending this constitutive law is to add elastic properties into it, like for example in the Maxwell fluid, where the stress also depends on how it changes with time (Astarita and Marrucci, 1974).

The main interest of application of the constitutive law is in the MIZ ice dynamics. There has been some controversy over the importance of the internal ice stresses on the ocean dynamics. The proposed constitutive law suggests that for the typical MIZ ice compactness values, from 0 to 85 (90)%, the pressure and the shear viscosity are negligible. Thus the internal ice stress does not contribute much to the ice dynamics (of course the ice is still more viscous than the ocean). This conclusion may be reached from another point of view; the frictional effects are important only near boundaries and far in the open ocean the ice motion is free drift. This is also supported by findings of Thorndike and Colony (1982), who explain most of the ice motion (86% of the variance) as a balance between the stresses exerted by the atmosphere and ocean and the Coriolis force (free drift).

3.3 Scaling of the Dynamical Equations of the Ocean

In the following the forced motion is studied, which means that constant wind field is applied over the ice and the ocean. The aim of this section is to show what dynamical regimes the chosen parameters represent and what are the major balances in the vorticity equation. It is assumed that the ice edge is parallel to the x-axis and ice is covering the positive y-axis side, the "northern" side. For a constant wind field the variation in the ice cover can introduce mesoscale effects. An across ice-edge change in surface stress leads to up/down-welling, but also a variation along the ice-edge direction can lead to up/downwelling enhancements.

The moving ice cover will manifest itself as a time dependent forcing for the ocean in the case where the ice cover varies in the ice-edge direction. For this reason the scaling is done in a coordinate system that moves with the speed of the ice, which is assumed constant (not quite true near the ice edge). The advantage is that the Ekman velocities will be time-independent.

In the coordinate system moving with speed c, the governing equations for the ocean are :

$$u_t + u\,u_x + v\,u_y = f_o v + \tau^x(x,y)/\rho h - g^* h_x \qquad (3.3.1)$$

$$v_t + u\,v_x + v\,v_y = -f_o\,(u + c) + \tau^y(x,y)/\rho h - g^* h_y \qquad (3.3.2)$$

$$h_t + (hu)_x + (hv)_y = 0, \qquad (3.3.3)$$

where $\tau(x,y)$ includes both the surface and the interfacial stresses. The velocity components are scaled by U, time by T, x and y by L, which is also the scale of variation in ice concentration. Two Rossby numbers are assigned $\bar{\varepsilon} = c/f_0L$, and $\varepsilon = U/f_0L$, the stratification parameter is $s = g^*H/f_0^2L^2$, parameter of the local acceleration is $\omega = 1/f_0T$. The forcing is scaled by $\tau_0/\rho H$, where H is the scale for the upper layer depth. With these conventions the x-momentum equation becomes

$$\omega\varepsilon u_t + \varepsilon^2(uu_x + vu_y) = \varepsilon v + (\tau_0/\rho f_0^2 HL)\tau_x/h - (g^*\eta/f_0^2L^2)h_x \qquad (3.3.4)$$

where η is the scale for interface change). To get a proper balance between the Coriolis term, the forcing and the pressure gradient, the following choice is made:

$$\tau_0/\rho f_0^2 HL = \varepsilon \text{ which leads to } U = \tau_0/\rho f_0 H \text{ and}$$
$$g^*\eta/f_0^2L^2 = \varepsilon \text{ which gives } \eta = \tau_0 L/g^* H\rho = H\varepsilon/s.$$

The scaled y-momentum equation is

$$\omega\varepsilon v_t + \varepsilon^2(uv_x + vv_y) = -\varepsilon u - \bar{\varepsilon} + \varepsilon\tau_y/h - g^*\eta'/f_0^2L^2)h_y \qquad (3.3.5)$$

If $\bar{\varepsilon} >> \varepsilon$ which means that for proper balance $g^*\eta'/f_0^2L^2 = \bar{\varepsilon}$, then $\eta' = cLf_0/g^* = H\bar{\varepsilon}/s$. As a consequence of this and the earlier

conclusion h can be divided into three parts:

$h = H(1 + (\bar{\varepsilon}/s)\bar{\eta} + (\varepsilon/s)\eta)$, where $\bar{\eta}$ is the interface change that supports the velocity c.

The velocities can be expressed now as a sum of geostrophic, Ekman and ageostrophic parts:

$$u = u_g + u_E + u_a = -\eta_y + u_E + O(\varepsilon) \qquad (3.3.6)$$

$$v = v_g + v_E + v_a = \eta_x + v_E + O(\varepsilon). \qquad (3.3.7)$$

When the velocities and h are substituted into the continuity equation, it becomes

$$\omega\eta_t + (s + \bar{\varepsilon}\bar{\eta} + \varepsilon\eta)\underline{\nabla} \cdot \underline{U}_E + \varepsilon u_E\eta_y + \varepsilon v_E\eta_y + \bar{\varepsilon}(v_E + \eta_x)\bar{\eta}_y = 0. \qquad (3.3.8)$$

where $\underline{U}_E = (u_E, v_E)$. Choosing c is to be negative, we have $\bar{\eta}_y = 1$ and $\bar{\eta} = y$, and then

$$\omega\eta_t + \bar{\varepsilon}\eta_x + (s + \bar{\varepsilon}y + \varepsilon\eta)\underline{\nabla} \cdot \underline{U}_E + \varepsilon\, \underline{U}_E \cdot \underline{\nabla}\eta + \bar{\varepsilon}v_E = 0. \qquad (3.3.9)$$

This equation states that the vortex tube stretching is balanced by steady translation of the wave pattern (2nd term), Ekman pumping (3rd term), translation due to Ekman velocities (4th term) and a forcing term due to the moving coordinate system (the last term). If the ageostrophic effects are taken into account (in eqs. 3.3.6 and 3.3.7) the vorticity equation is in full:

$$\omega\eta_t + \bar{\varepsilon}\eta_x + (s + \bar{\varepsilon}y + \varepsilon\eta)[\underline{\nabla} \cdot \underline{U}_E - \omega\nabla^2\eta_t - \varepsilon J(\eta, \nabla^2\eta + \hat{k} \cdot \underline{\nabla}x\underline{U}_E)$$

$$-\varepsilon\underline{\nabla} \cdot ((\nabla^2\eta + \hat{k} \cdot \underline{\nabla}x\underline{U}_E)\underline{U}_E)] + \varepsilon\underline{U}_E \cdot \underline{\nabla}\eta - 1/2\varepsilon\omega|\nabla\eta|^2_t - 1/2\varepsilon^2(J(\eta, |\nabla\eta|^2)$$

$$+ \underline{U}_E \cdot \underline{\nabla}|\nabla\eta|^2) - \varepsilon^2(\eta_x J(\eta, v_E) - \eta_y J(\eta, u_E) + \eta_x \underline{U}_E \cdot \underline{\nabla}u_E) + \bar{\varepsilon}v_E - \bar{\varepsilon}\omega\eta_{yt}$$

$$- \bar{\varepsilon}\varepsilon(J(\eta, \eta_y) + \underline{U}_E \cdot \underline{\nabla}\eta_y - J(\eta, u_E) - \underline{U}_E \cdot \underline{\nabla}u_E) = 0 \qquad (3.3.10)$$

To second order the essential terms are the advection of the relative and wind induced vorticity, the 5th and 6th terms.

The typical ice concentration variation near the ice edge is order of 10-30 km, which defines the scale of motion, L ~10^4m. In the case of a thick upper layer, h ~ 100 m (g^*=0.0198 ms^{-1}), the stratification parameter s is of O(1) (f_o ~1.4 $10^{-4}s^{-1}$). The Ekman velocities of the ocean are very slow compared to ice velocities, which corresponds to $\bar{\varepsilon}$>>ε. The vorticity equation for this system reduces to:

$$\omega(\eta_t - \bar{\varepsilon}\eta_{yt} - (s + \bar{\varepsilon}y)\nabla^2\eta_t) + \bar{\varepsilon}\eta_x + (s + \bar{\varepsilon}y)\underline{\nabla} \cdot \underline{U}_E + \bar{\varepsilon}v_E = 0,$$

where ω is the largest of O(ε,s). This equation reduces further if we take into account that for typical values of c ~.3 ms^{-1}, L ~ 10^4 m and U ~0.05 ms^{-1}, the Rossby numbers are $\bar{\varepsilon}$ ~ 0.2 and ε ~ 0.03. Thus

$$\omega\,(\eta_t - s\,\nabla^2\,\eta_t) + s\,\underline{\nabla}\cdot\underline{U_E} = 0 \qquad (3.3.11)$$

This equation represents linear dynamics and it gives a linear change in the depth of the pycnocline due to the Ekman pumping.

For the thin upper layer case ($h = 25$ m, $g^* = 0.0172\ ms^{-2}$) and for length scales of order of 10^4 m, the stratification parameter is $s \sim 0.25$. Because the winds act on a much shallower water body, the velocities in the ocean are expected to be of the same magnitude as in the ice, so that $\bar{\varepsilon} \sim \varepsilon \sim s \sim 0.25 \ll 1$. For this parameter range the vorticity equation (3.3.10) reduces to

$$\omega\eta_t + \bar{\varepsilon}\eta_x + (s + \bar{\varepsilon}y)\underline{\nabla}\cdot\underline{U_E} + \varepsilon\underline{\nabla}\cdot(\eta\underline{U_E}) + \bar{\varepsilon}v_E = 0, \qquad (3.3.12)$$

where ω is the largest of $O(s,\bar{\varepsilon},\varepsilon)$. If there is no Ekman pumping (3rd term) the solution reduces to steady translation of the interface. The 4th term gives the advection of the wave pattern due to the Ekman velocity. It is the main nonlinear interaction. Compared to the linear eq. (3.3.11) this term gives highly asymmetric behaviour of the nonlinear system when the forcing (Ekman transport) is time-dependent.

For the longer time scales the evolution of the vorticity equation is governed mainly by dispersion. For $\bar{\varepsilon} \gg \varepsilon$ the next order equation is of $O(\bar{\varepsilon}\varepsilon, \varepsilon, s\varepsilon)$ and for $\bar{\varepsilon} \sim \varepsilon$, it is of $O(s\varepsilon, \bar{\varepsilon}\varepsilon, \varepsilon^2)$ which both represent time scales 5 to 10 days. If the forcing has

time scales smaller than this, then motion is essentially governed by equations (3.3.11) and (3.3.12).

If the scale of variation of the ice cover in the x-direction (along ice edge) is smaller than the scale in y-direction, the dynamics of the ocean hardly resolves it. On the other hand, if the x-scale is very large, the equations are also x-independent. This leads to the conclusion that forced motion can exist only in a limited band of wavelengths. The smallest x-scales are 2-3 times the Rossby radius of deformation, but more typically 4-5 times R_d, which is the scale of variation in ice concentration in the across ice edge direction.

4. Up/downwelling at the Ice Edge

4.1 Linear and Nonlinear Dynamics

Upwelling at the ice edge has been extensively studied by Roed and O'Brien (1981),(1983). This section is mainly a review of the simple balances in the dynamical equations that lead to up/downwelling. To describe the physics, only cases of the strongest up/downwelling signal are considered in the following. The largest response occurs when the ice edge does not move, which happens for slightly off-ice winds, about 30° from ice edge (Smedstad and Roed, 1984). The small off-ice component of wind is needed to cancel the ice drift due to the oceanic Ekman velocity.

In the following we study the simplified one-dimensional equations (no y-derivatives). (In the velocity components, index i refers to ice, oceanic quantities have no indeces)

$$u_{i,t} = f_o v_i + \tau_x^{ai}/\rho_i D - \tau_x^{iw}/\rho_i D \qquad (4.1.1)$$

(D=constant ice thickness)

$$v_{i,t} = - f_o u_i + \tau_y^{ai}/\rho_i D - \tau_y^{iw}/\rho_i D \qquad (4.1.2)$$

$$A_t = - (Au_i)_x \qquad (4.1.3)$$

$$u_t = f_o v - g^* h_x + (1 - A)\, \tau_x^{aw}/\rho_w H + A\tau_x^{iw}/\rho_w H \qquad (4.1.4)$$

$$v_t = - f_o u + (1 - A)\tau_y^{aw}/\rho_w H + A\tau_y^{iw}/\rho_w H \qquad (4.1.5)$$

$$h_t = - Hu_x \qquad (H = \text{the undisturbed thickness of the upper layer}) \qquad (4.1.6)$$

As discussed earlier in section 4.2 the internal ice stresses are negligible for the typical MIZ ice concentrations (< 85 %), which means that the ice motion is essentially described by free drift. The steady state solution for the ice is given approximately from (4.1.1) and (4.1.2) as

$$\rho_a C_{ai} W^2 = \rho_w C_{wi}(v_i - v)^2 \approx \rho_w C_{wi} v_i^2, \qquad (4.1.7)$$

where W=wind speed. With chosen parameters

$v_i \sim \sqrt{\rho_a C_{ai}/\rho_w C_{wi}}\, W \approx 2\%$ of the wind speed,

$u_i \sim 0$ because of the chosen wind direction, 30^o off the ice edge.

The 2% drift factor is twice the experimental values of 0.8-1.2%, even though this number is computed with very large $C_{wi} = 10 \cdot 10^{-3}$ and $C_{ai} = 3.6 \cdot 10^{-3}$. Changing C_{ai} to be $3 \cdot 10^{-3}$ still gives a drift factor of 1.9%. In the following calculations $C_{iw} = .01$ or .015 has been used, but the results do not change much by varying C_{iw} from $5.5 \cdot 10^{-3}$ to $15 \cdot 10^{-3}$.

The oceanic velocities are from eqs. (4.1.4) and (4.1.5):

$$v = g^* h_x/f - (1 - A)\tau_x^{aw}/\rho_w H - A\tau_x^{iw}/\rho_w H, \qquad (4.1.8)$$

$$u = (1 - A)\tau_y^{aw}/\rho_w H + A\tau_y^{iw}/\rho_w H, \qquad (4.1.9)$$

which lead to a linear increase (or decrease) in time of the

pycnocline depth. The effect of the chosen parameters, $C_{ai} \approx 2\text{-}3$ C_{aw} and large C_{iw}, is that the wind parallel to ice edge, ice on the right, produces upwelling. This happens because the momentum flux from the air to ice and from ice to ocean is much larger than flux from air to ocean, which gives bigger Ekman transport underneath the ice than in the open ocean. The width of the upwelling zone is determined by the gradient (scale of variation) in the ice concentration (assuming that the ice edge does not move much). If the ice edge is sharp, like a step-function, the scale is the baroclinic radius of deformation. If the ice edge moves considerably during the wind event, the upwelling zone is very weak and the width is determined by the distance that the ice travelled.

In figures (6) and (7) the pycnocline height anomalies, ice concentrations and oceanic velocities are shown for thick and thin upper layer cases after five days of upwelling favorable wind W = 10 m/s inclined 30° off the y-axis. The former resembles the wintertime and the latter the summertime conditions in the Greenland Sea where the baroclinic radii are 10 km (H=100 m) and 4.6 km (H=25 m) respectively. The one-dimensional model area was 200 km wide (grid size 1 km). The figures show that the open boundaries at x=0 and x= 200 km are well behaved. The ice edge located initially at x= 100 km. The ice thickness is constant, 4 m, unless otherwise stated.

When the upper layer is thin, the pycnocline changes can easily become comparable to the layer thickness, leading to nonlinear

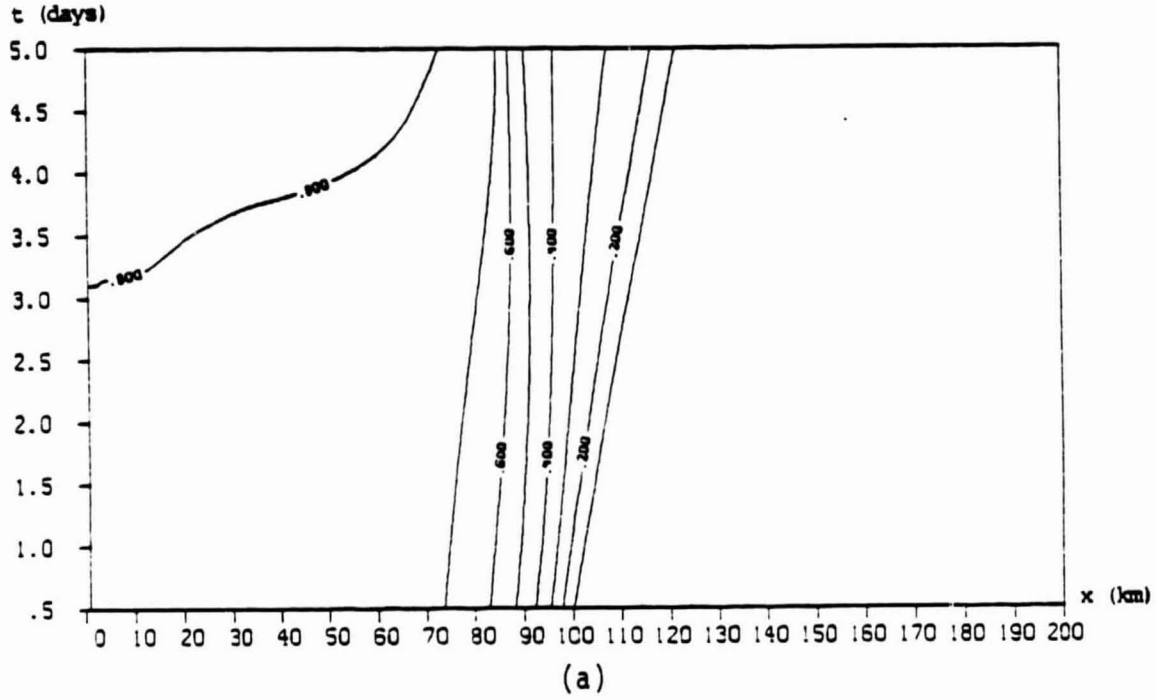

Figure 6. The x-t plots of the ice concentration (a), the pycnocline anomaly (b) (contours in meters), u-velocity (the across ice edge component) (c) and v-velocity (along the ice edge component (d). Velocity contours are in cm/s. In this case the undisturbed upper layer thickness is 100 m. The wind is 10 m/s and inclined 30° away from the ice edge (ice on the right).

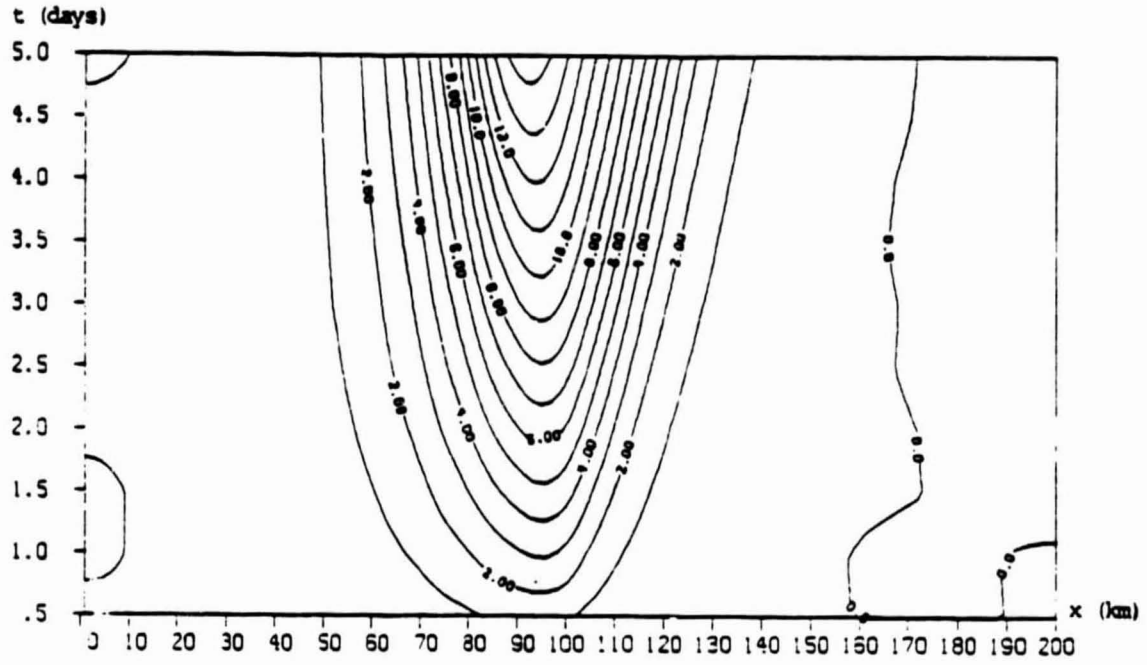

Figure 6 (b).

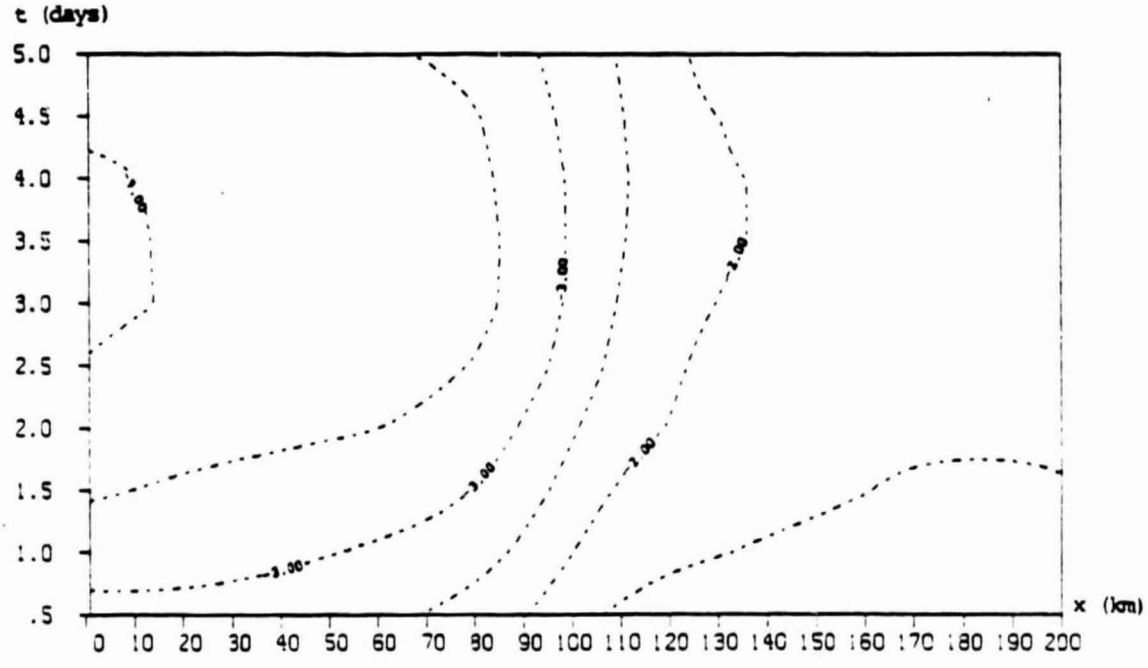

Figure 6 (c).

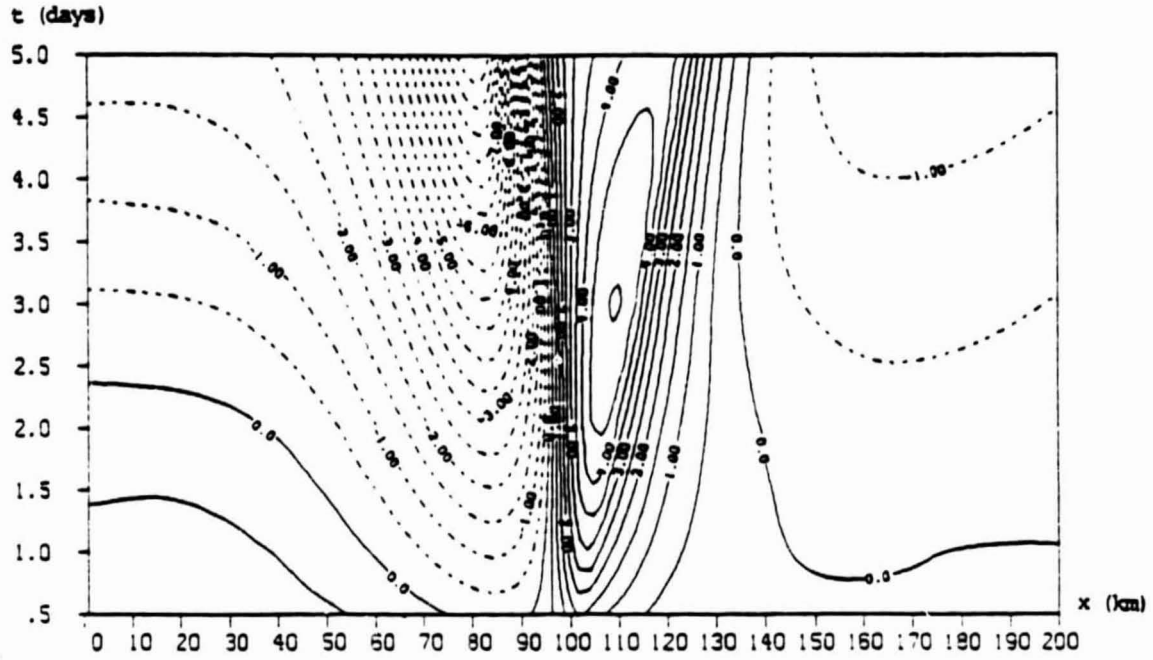

Figure 6 (d).

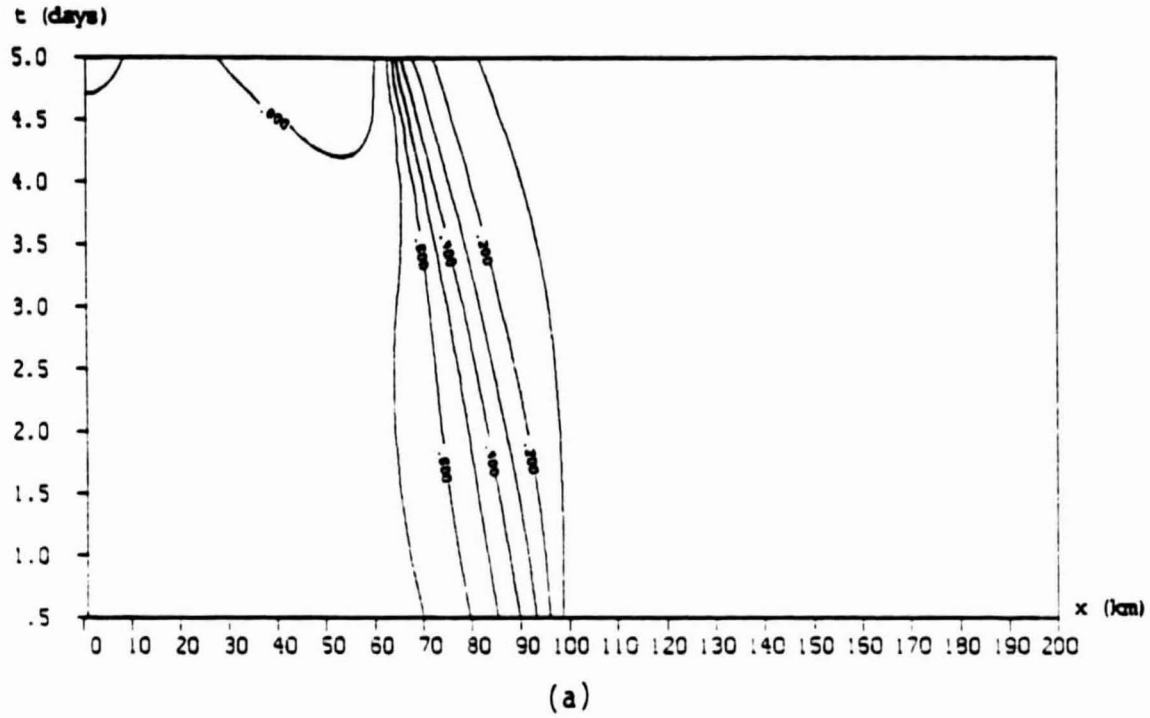

(a)

Figure 7. The x-t plots for case H = 25 m, (a) the ice concentration, (b) the pycnocline anomaly (in m), (c) and (d) are u- and v-velocities (in cm/s). The forcing is the same as in figure 6.

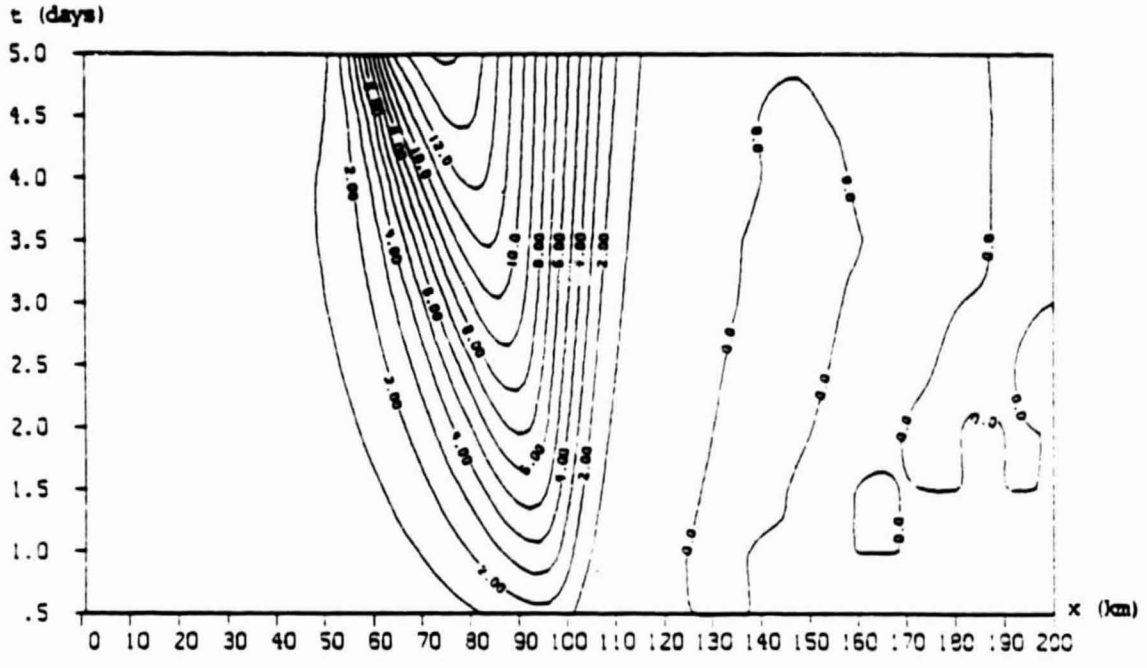

Figure 7 (b).

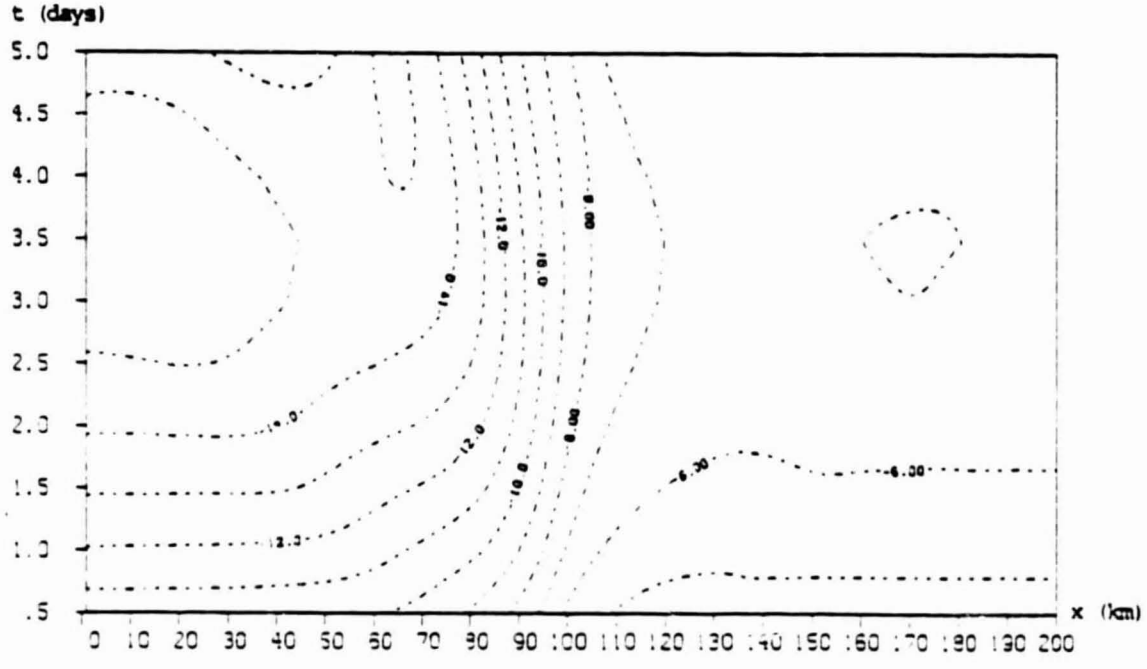

Figure 7 (c).

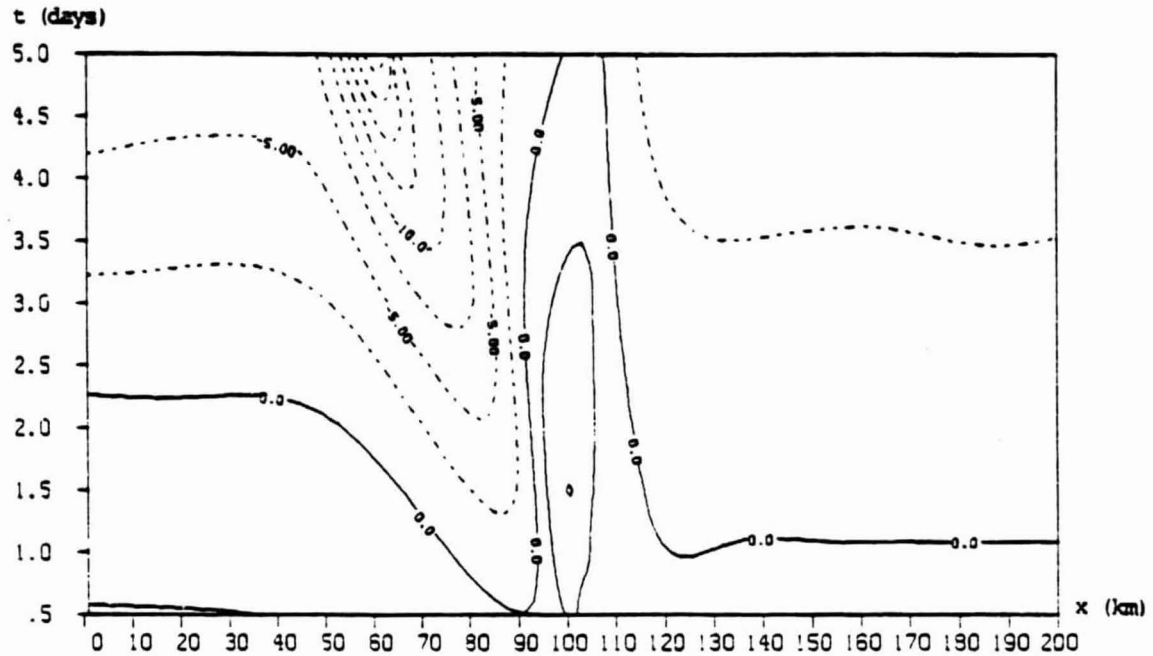
t (days)
5.0
4.5
4.0
3.5
3.0
2.5
2.0
1.5
1.0
.5
0 10 20 30 40 50 60 70 80 90 100 110 120 130 140 150 160 170 180 190 200
x (km)
5.00
10.0
0.0

Figure 7 (d).

dynamics. This is demonstrated by comparing figures (6b) and (7b) showing the pycnocline height anomaly in linear (H=100 m) and in nonlinear (H=25 m) cases. The nonlinearity causes an asymmetry in the upwelling signal. For longer wind events the steeper side will shift under the ice compared to the earlier stages of the upwelling, and the opposite is true for downwelling. This frontal formation is caused by the advection of the pycnocline perturbation and of the relative and the wind induced vorticity by the Ekman velocity, the sixth and seventh terms in equation (3.3.10). This asymmetry is well seen in the observations of Johannessen et al. (1983) (figure 10).

In the thicker upper layer case the ice edge moves towards positive x-direction with the wind inclined 30° from the ice edge, because the Ekman velocity is too small to cancel the ice motion (due to wind) in x-direction. As a general feature the divergence in the oceanic velocities affect the ice velocities so that they tend to smooth the gradient of the ice concentration near the edge during the first couple of days of the upwelling event.

In the thin upper layer case the ice edge converges strongly (even stronger convergence of the ice edge happens in a nonlinear downwelling case). The convergence of the ice edge (figure 7) is connected to the formation of the very strong upwelling jet due to the formation of the front. The oceanic jet is forcing the ice to move faster at the edge than further out in the ice pack. This

variation gives a feedback to the oceanic velocities, giving rise to a local minimum in the Ekman transport (figure 7c) near the edge. This in turn is reflected in the x-(across the ice edge) velocity component of the ice (figure 8); thus the ice is forced to converge near the edge.

Figure (8) shows the ice velocities when the upper layer is thin at day 3 and 5. In the beginning of the upwelling event the "jet" like enhancement is not very pronounced. The oceanic velocity structure is clearly reflected in the ice velocities. The profile at day 3 shows enhancement of the along ice edge component of 30% near ice edge, falling short of the reported values; e.g. 100% from Johannessen et al. (1983). The situation though changes after a few days, and at day 5 the jet feature is very pronounced, with a maximum of twice the speed further in the ice pack.

The essential requirement for the formation of a strong upwelling pattern and jet is to have a mechanism to keep the ice edge sharp, i. e. to cancel the smoothing coming from the oceanic divergence effect on ice. Next an initial condition of a step-function like ice concentration is considered. The thickness of the ice varies from 6 m far away from the ice edge to 0 meters at the edge, the ice concentration being 100% for all times. For this case only the continuity equation (3.1.4) needs to be solved. This geometry will produce a strong pycnocline response and hence a strong ice edge jet figure (9) in one day of upwelling favorable wind of 10 ms^{-1}.

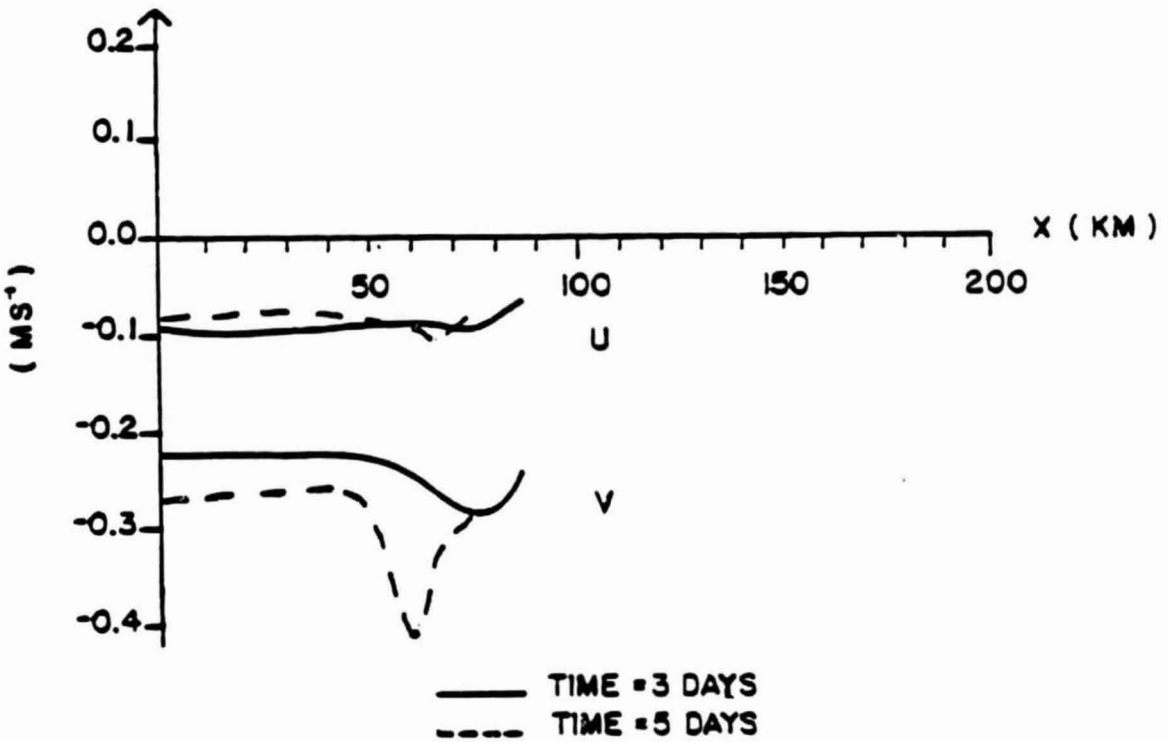

Figure 8. Ice velocities corresponding to figure 7.

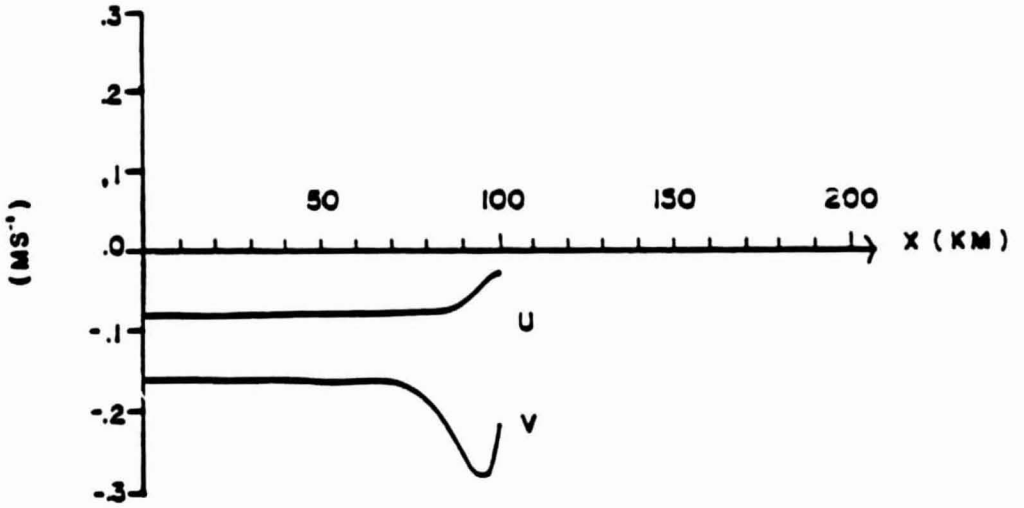

(a)

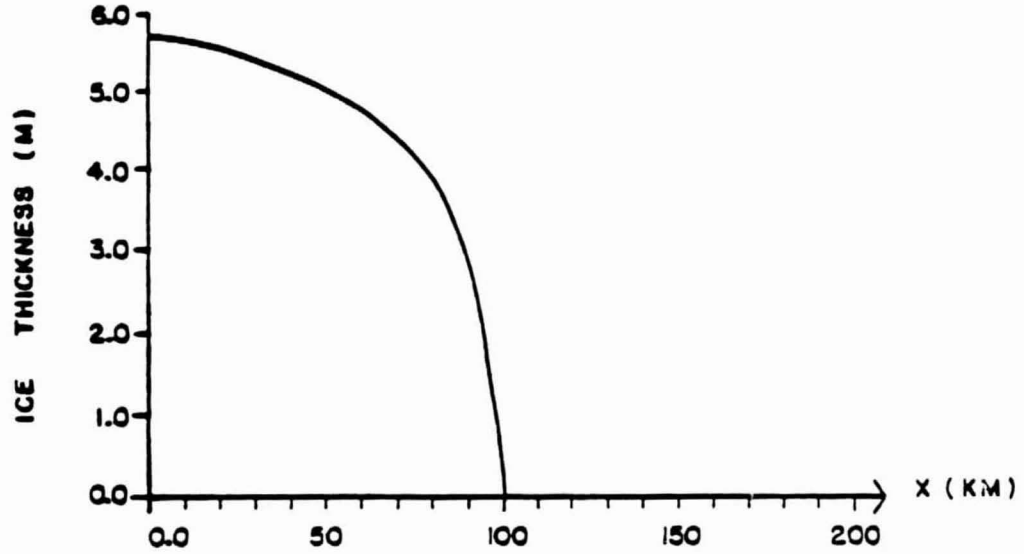

(b)

Figure 9. Ice velocities (a), when ice compactness is 100 % and ice thickness (b) varies, after one day of upwelling (H = 25 m). Winds are 10 m/s.

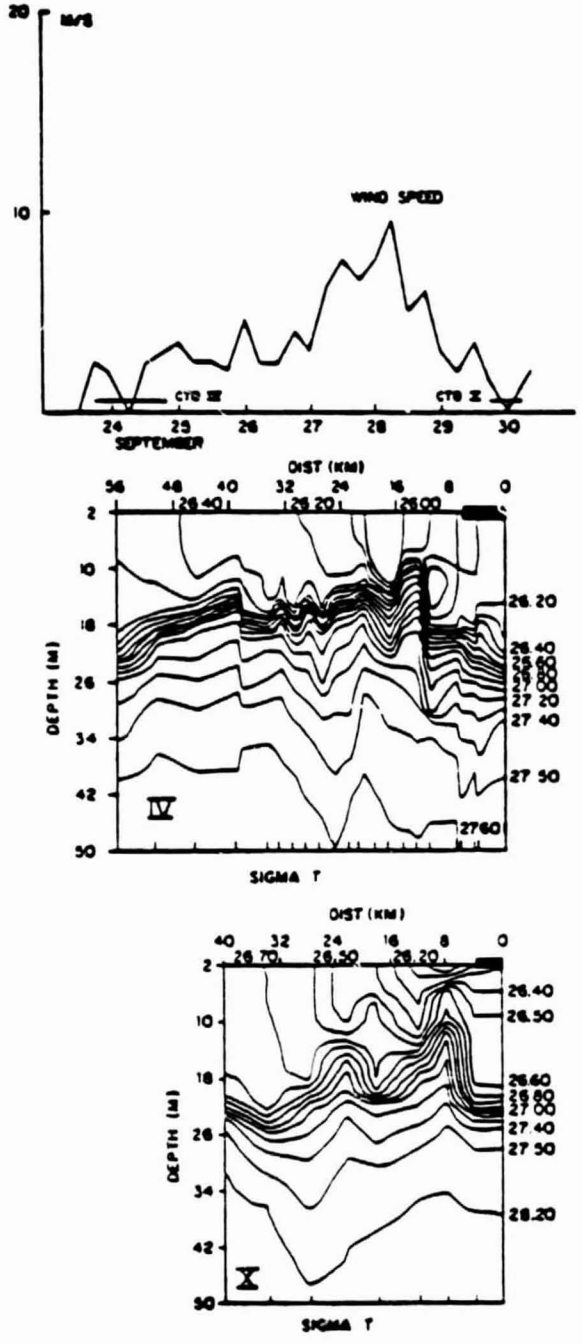

Figure 10. Hydrographic sections near the ice edge in the Greenland Sea in early Fall 1979. From Johannessen et al. (1983).

The effect of varying ice thickness is negligible due to the high interfacial stress coefficient as seen from figures (9a) and (9b). The strong velocity enhancement comes again from the oceanic upwelling jet.

4.2 Stability of the up- and downwelling jets

The barotropic instability of the computed up-and downwelling jets is considered. The stability analysis for the forced system is very complicated (or nearly impossible) so the problem is simplified to study only the instability of the geostrophic velocity component calculated from the interface changes. This approach can be justified by looking at the gradients of the potential vorticity for the forced upwelling system and for its geostrophic counterpart, as in figures (11a) and (11b), which show extreme resemblance with each other. The stability of the jet is examined at its different stages of development. For example, we compute the stability of the jet after it had been forced for 3 days, after which the winds relax. Without external forcing the deformation of the interface and the corresponding geostrophic jet will be preserved because frictional effects are negligible.

To study the stability problem we start from the potential vorticity equation for the basic state

$$\frac{d}{dt}\ \Pi_B = \frac{d}{dt}\frac{f+\xi}{h} = 0 \qquad \left(\frac{d}{dt} = \frac{\partial}{\partial t} + U\frac{\partial}{\partial x} + V\frac{\partial}{\partial y}\right) \tag{4.2.1}$$

where $\xi = V_x$, the relative vorticity , $U = 0$, $V = g^* h_x/f$, U and V are

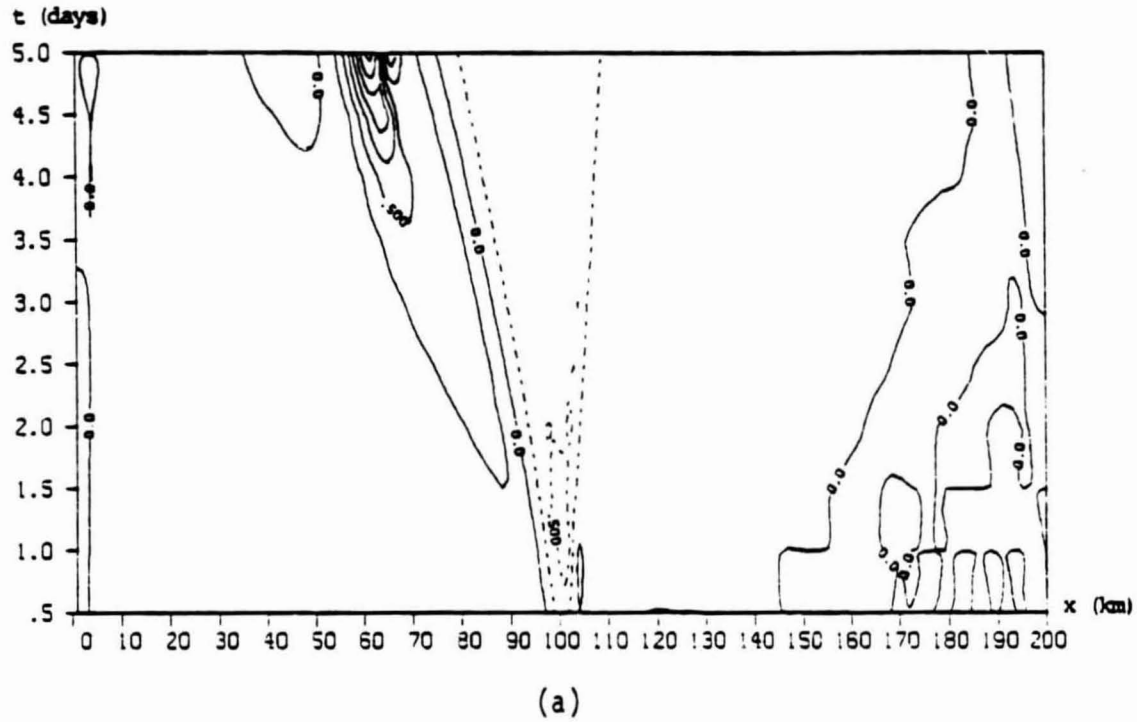

(a)

Figure 11. Potential vorticity gradient (multiplied by the thickness of the upper layer) during the 5 days of (a) upwelling, H = 25 m, (b) upwelling (H = 25 m), but only the geostrophic part of v is included, (c) downwelling, H = 25 m. The contour units are 10^{-8} m^{-1} s^{-1}. In cases (a) and (b) the forcing is the same as in figures 6 and 7, in (c) the winds are reversed.

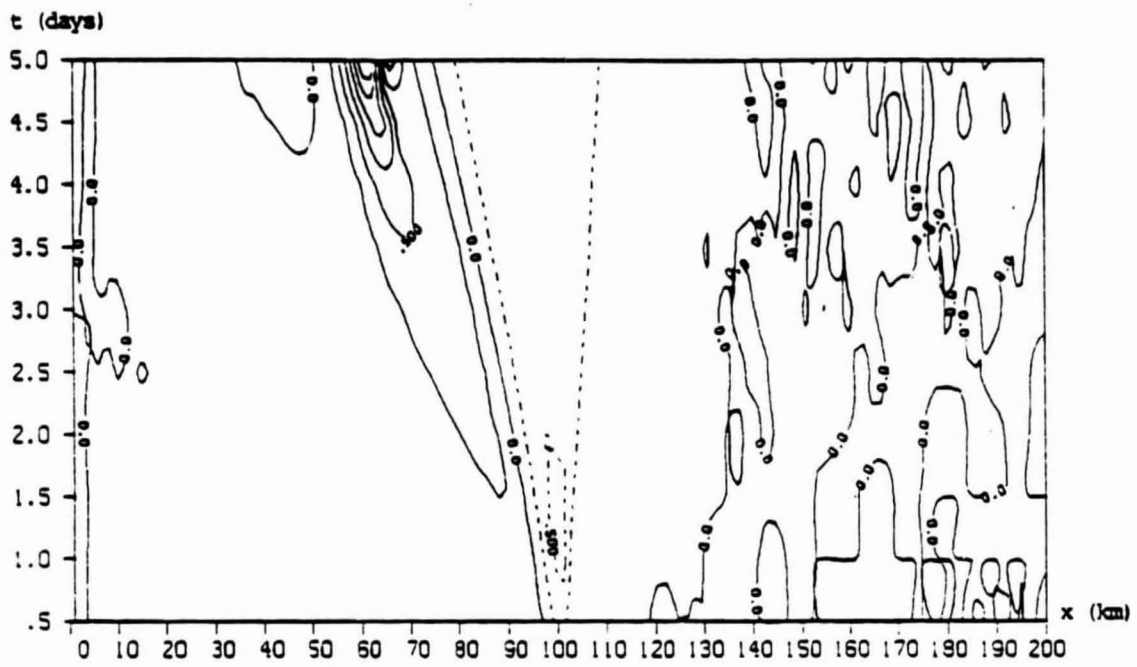

Figure 11 (b).

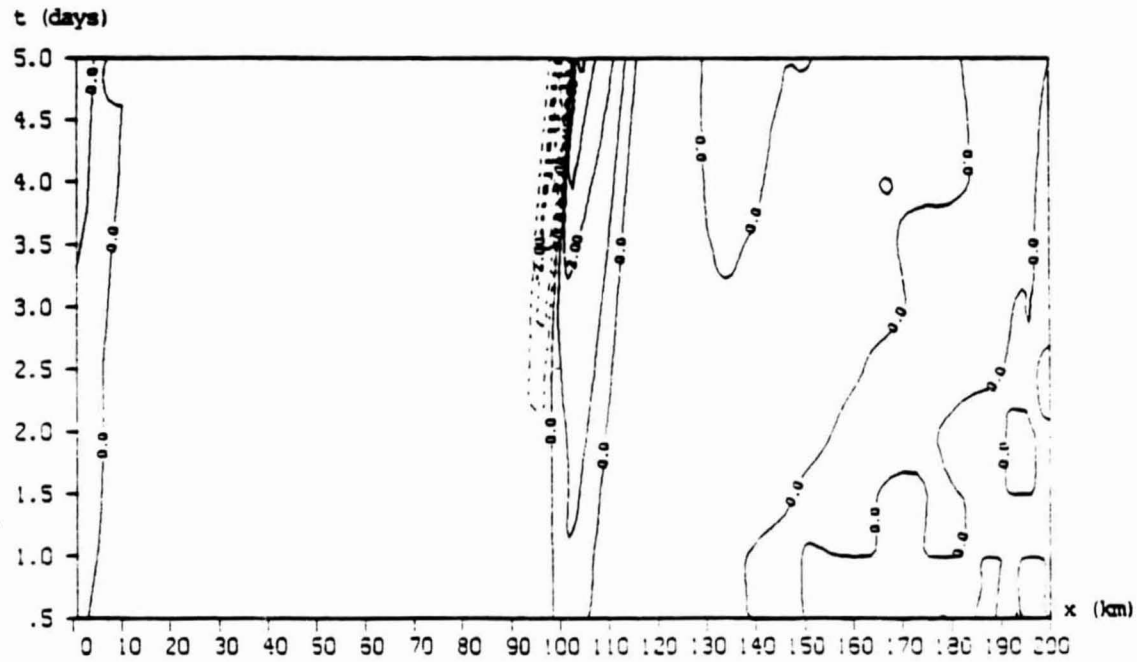

Figure 11 (c).

the mean flow velocity components. To get the vorticity equation of the perturbed flow we replace U by $u'(x,y,t)$, V by $V(x) + v'(x,y,t)$, h by $h(x) + h'(x,y,t)$ and ξ by $\xi(x) + \xi'(x,y,t)$ (the primed quantities refer to the perturbed state). It is assumed that e-folding times are large compared to the perturbation, so that the jet can be treated as quasi-stationary, i. e. the basic state is time independent. The validity of this statement can be reconsidered after computations. But, until we find out the e-folding times, we assume that the jet was not destroyed by any prior instability.

The vorticity equation is, after linearization (dropping terms like $u'\xi'$ etc.) :

$$\left(\frac{\partial}{\partial t} + V \frac{\partial}{\partial y}\right) \xi' - \left(\frac{f+\xi}{h}\right) \left(\frac{\partial}{\partial t} + V \frac{\partial}{\partial y}\right) h' + hu' \frac{\partial}{\partial x} \frac{f+\xi}{h} = 0 \qquad (4.2.2)$$

When the geostrophic approximation is applied for the perturbation velocities, the equation becomes:

$$\left(\frac{\partial}{\partial t} + V \frac{\partial}{\partial y}\right) \nabla^2 h' - (f \Pi_B / g^*) \left(\frac{\partial}{\partial t} + V \frac{\partial}{\partial y}\right) h' - h \Pi_{B,x} h'_y = 0 \qquad (4.2.3)$$

Inserting the Fourier decomposition $h'(x,y,t) = \phi(x) e^{i(ky-\omega t)}$ gives

$$\phi'' - (k^2 + f^2/g^* h) \phi - (h\Pi_{B,x}/(V - \omega/k)) \phi = 0, \ \phi(\pm \infty) = 0. \qquad (4.2.4)$$

For small Rossby number ($\xi << f$) $h\Pi_{B,x} = V'' - f^2 V/g^* h$. The equation (4.2.4) is essentially modified Rayleigh equation which is known to have unstable eigenfunctions if the gradient of potential vorticity (of the basic state) $\Pi_{B,x}$, vanishes at some point (Lin,

1955; Stern, 1961). The plots for time evolution of the potential vorticity gradient of the upwelling system show that the flow is more unstable in the beginning of the upwelling and after 4 days of upwelling. The latter instability can be associated with the frontal formation. The potential vorticity gradient of a downwelling system (figure 11c), show increasingly positive and negative regions implying stronger instability than in the upwelling case. In the limit of small Rossby number, Stern (1961) showed that for a given velocity profile there must exist a maximum critical depth $(H_\infty)_{cr}$ above which the mean flow is unstable: $0 < f^2/g^*(H_\infty)_{cr} < \max V''(x)/V(x)$. This means that, in our particular case, the downwelling jet is always more unstable than the upwelling one.

The equation (4. 2.4) was solved numerically for the given geostrophic velocity profiles. The growth rates for all computed cases are plotted in figure 12. During the first two days of upwelling the interface changes are not large. Both terms in $\Pi_{B,x}$ support strongly the sign change so that there is one unstable mode. The wavelength of the most unstable eigenfunction shifts towards larger scales as time increases so that at day 3 the flow is nearly stable. Unstable modes are again introduced to the system when the front forms after day 4. The phase velocities change sign also going from day 2 to day 5, the propagation direction being that of the stronger branch of the jet. The frontal instability is still quite weak with maximum e-folding time of about 7 days compared to the

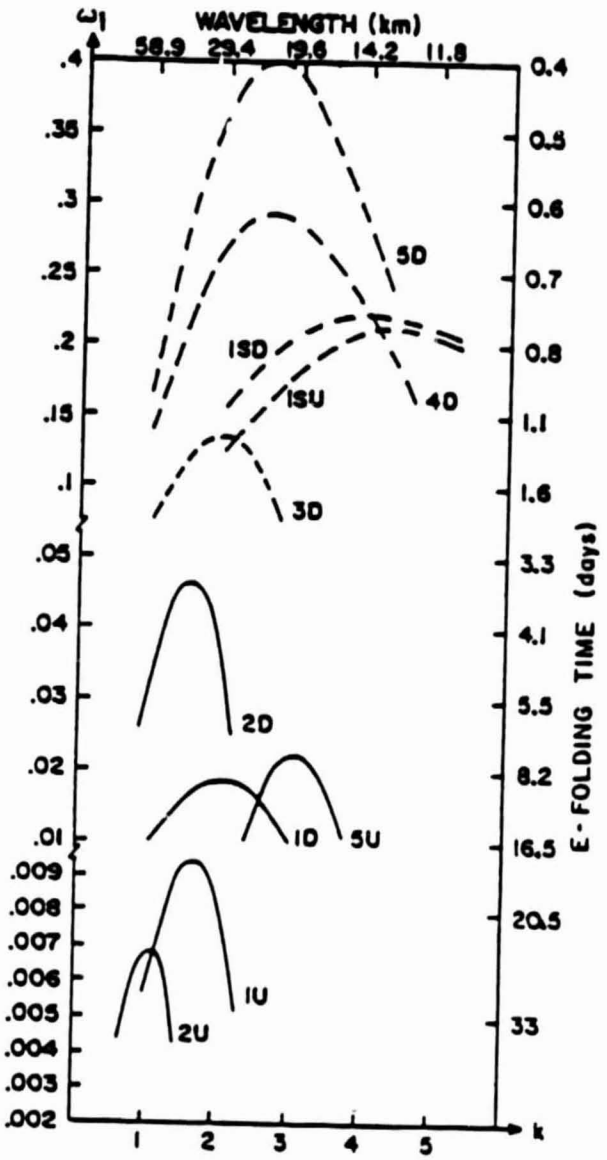

Figure 12. The growth rates of the up- and downwelling jets after different periods of forcing. U=upwelling, D=downwelling, ND refers to downwelling jet at day N. 1SU and 1SD refer to to up- and downwelling jets at day 1, when the ice edge is a step-function.

growth rates of the downwelling jet, which has an e-folding time at day 5 of 0.4 days. In the latter the most unstable wavelength asymptotes to 22 km in the later stages of downwelling. Considering the assumption of a quasi-stationary jet, the computations for the downwelling jet at day 3, 4 and 5 are unrealistic (which is the reason that they are marked with dashed lines). In these cases the e-folding times are of the same order or less than the time required to develop the jet.

The above up- and downwelling profiles were computed for a moderate ice concentration gradient. When the ice edge is a step function, the ocean response is limited to a narrow region, leading to very strong shears. The stability of the up- and downwelling jets after one day of forcing are also shown in figure 12. The e-folding times of the steady jet are nearly the same as the forcing time, which seems to suggest nearly immediate disintegration of the jet.

This analysis has demonstrated that the unstable wavelengths depend strongly on the ice concentration gradient, which can vary from 12-14 km up to around 100 km. For moderate ice concentration gradients the most unstable wavelength is 20-30 km. Due to the divergence term, the downwelling jet is far more unstable barotropically than the upwelling jet. The growth rates for the upwelling jet at different stages are so small that the jet can be considered nearly stable if the ice concentration gradient at the edge is not very strong.

4.3 Ice Bands

Banding is a frequently seen phenomenon in the marginal ice zones. The observed band width varies strongly. The first observations from satellite pictures suggested the width to be around 10 km with nearly an equal amount of open water between them (Muench and Charnell, 1977). Later shipboard observations revealed even narrower band structure at the ice edge. Typically these bands are 500 m to 1 km wide, the length of these band features being a few kilometers (Bauer and Martin (1980)). The bands are usually seen with off-ice winds, with their long axis at 40°-90° to the left of the wind direction. However, in the above no references have been made to the wind conditions that prevailed before the actual observations. As we will show, the preceding wind conditions are important for band formation.

Many theories have been offered to explain ice banding. One of the theories offered by Wadhams (1983) suggests that the wave radiation pressure of the fetch-limited sea produced by the off-ice wind plays the major role in the band generation. In the initial state the ice cover has randomly distributed polynyas. The wave pressure is concentrated on the floes at the downwind end of each polynya and accelerates them towards the neighboring floes further downwind. Internal compacting stress and swell incident on the band from seaward will maintain the bands' integrity.

Another theory by Muench et al., (1980) suggests that there could be interactions between the internal waves and band formation, because the bands are found overlying a two-layer density structure. Furthermore, they show that the internal wave speeds and wave lengths are similar to the ice band speeds and spacings.

As seen from figure (10) from Johannessen et al. (1983), there are "wave" like features in the pycnocline. These have amplitudes of 3-8 meters and their width is about 5-8 km. In two of the σ_t sections it appears as they would exist in pairs. Mork (1983) has suggested that these "waves" are like lee-waves due to moving ice, the major assumption being that the ice moves faster than some of the first few baroclinic modes. It is his explanation that the ice bands form due to these lee-waves, which have the same wavelengths as the band widths.

All of the above mentioned theories are more or less suggestive, as none of them can actually show that they can produce the bands. It is quite doubtful that randomly distributed polynyas can suddenly reorganize into evenly spaced bands, Wadhams (1983) or that a propagating internal wave field will organize the ice floes into bands, Muench et al., 1983.

To see if these features are forced "waves" the model was run with spatially constant wind stress, sinusoidal in time with a period of four days. This experiment was designed to simulate successive cyclone passings. The results after three cycles (12 days) are shown

in figures (13) and (14) for a nonlinear (H = 25 m) and a linear (H = 100 m) case. The wind is inclined 30° away from the ice edge and its maximum magnitude is 12 m/s. The drag coefficients used are $C_{ai} = 3.6 \cdot 10^{-3} = 3 \times C_{aw}$, $C_{wi} = 10 \cdot 10^{-3}$.

In the nonlinear case two upwelling enhancements are formed during the 12 days, and this pair will tend to amplify with time. The nonlinearity in the form of advection of the wave pattern redistributes vorticity when Ekman transport varies with time. It is the major reason that the formed up- and downwelling responses do not disappear in wind reversals: Initially one upwelling signal is formed, after the wind changes this pattern moves away from the ice edge (due to the opposite Ekman transport) while a downwelling pattern is established at the edge. During the next wind change an upwelling signal starts to develop again but it will be weaker than the first one because it has to overcome the downwelling pattern trying to propagate underneath the ice.

The variation in the upper layer thickness will cause convergences and divergences in the oceanic velocities which are transferred to the ice velocities through the strong interfacial stress. Thus the oceanic dynamics induces band formation. Furthermore, from figure (13a) one sees that the deformation of the ice concentration will support the existence of this upwelling enhancement pair, thus maintaining the bands. The ice bands form only in the case of a thin upper layer, where the band development is

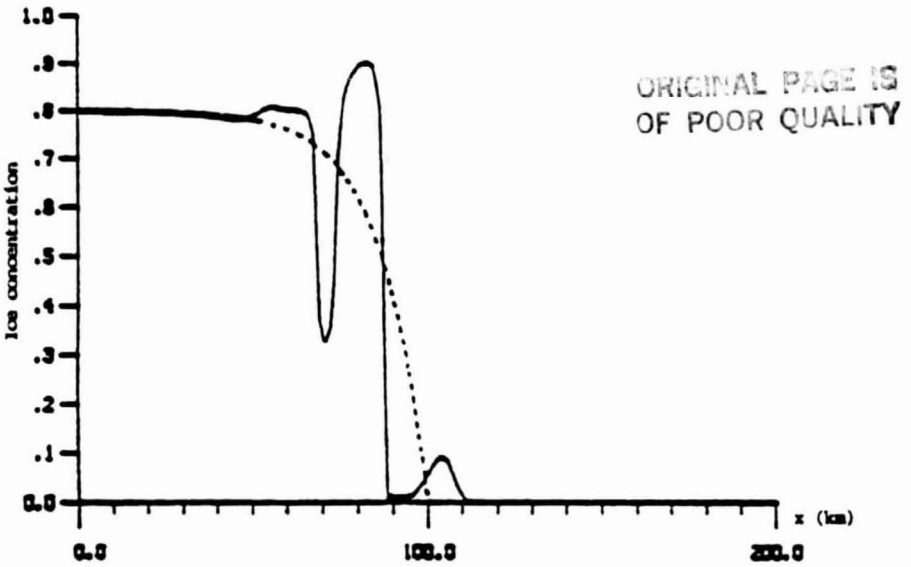

(a)

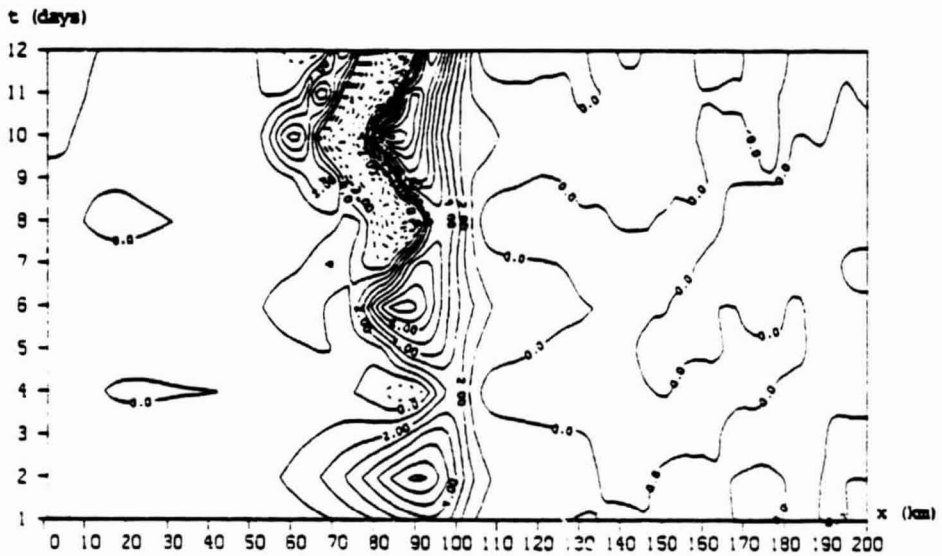

(b)

Figure 13. The ice concentration (a) after 3 cycles of sinusoidally varying wind stress (period = 4 days). (b) x-t plot of the pycnocline changes, contours in meters. In (a), the initial condition is shown with dashed line. The upper layer thickness is 25 m and the amplitude of the wind variation is 12 m/s.

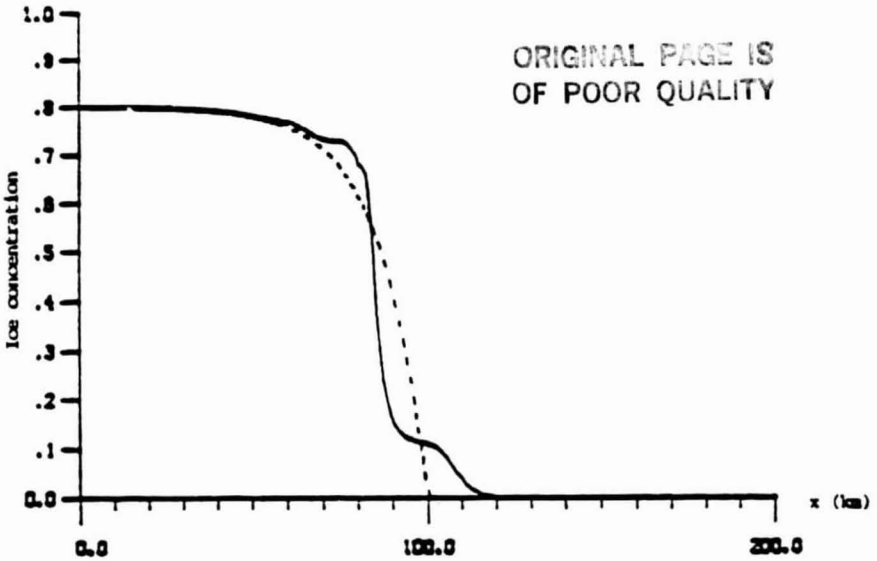

(a)

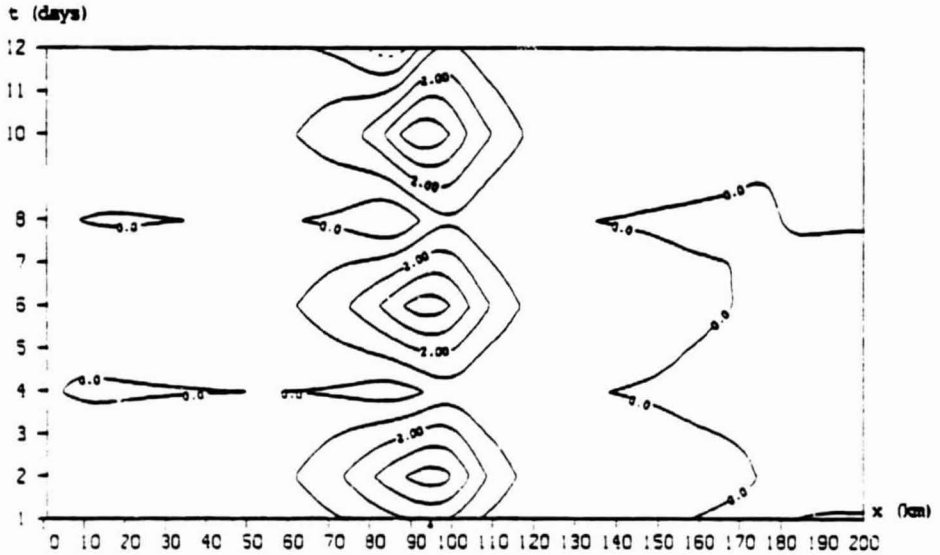

(b)

Figure 14. The same forcing as in the previous figure is applied, but for upper layer thickness 100 m. (a) is the ice concentration and (b) the x-t plot of the pycnocline anomaly (in meters). The initial condition is shown with dashed line in (a).

already evident after two cycles. For a thick upper layer there are neither ice bands or strong pycnocline changes, figure (14).

The simulated ice bands are 10-15 km wide, about 2-3 Rossby radius of deformation. After the innermost band is nearly separated there will be formation of new bands (and new "waves" in the pycnocline). If the ice is more mobile (smaller concentrations imply less resistance to convergence), the cyclone passings can effectively produce bands. Example of this is shown in figure (15) after 5 cycles (20 days).

Other model simulations show that the bands form more slowly if the period of wind forcing is less than 4 days. For shorter period forcing it takes a longer time to make the pycnocline changes strong enough that the Ekman velocities can affect the ice velocities. For longer period forcing only one wind reversal is needed to produce one band.

In order to explain that the ice bands are seen especially during off-ice winds, one sees from figure (13a) that the band structure is not clearly separated: The off-ice winds can separate the ice bands because the underlying upper layer structure will force the bands to move faster than the rest of the ice pack. This happens during the first few hours of off-ice winds and before the Ekman flow is established in the ocean.

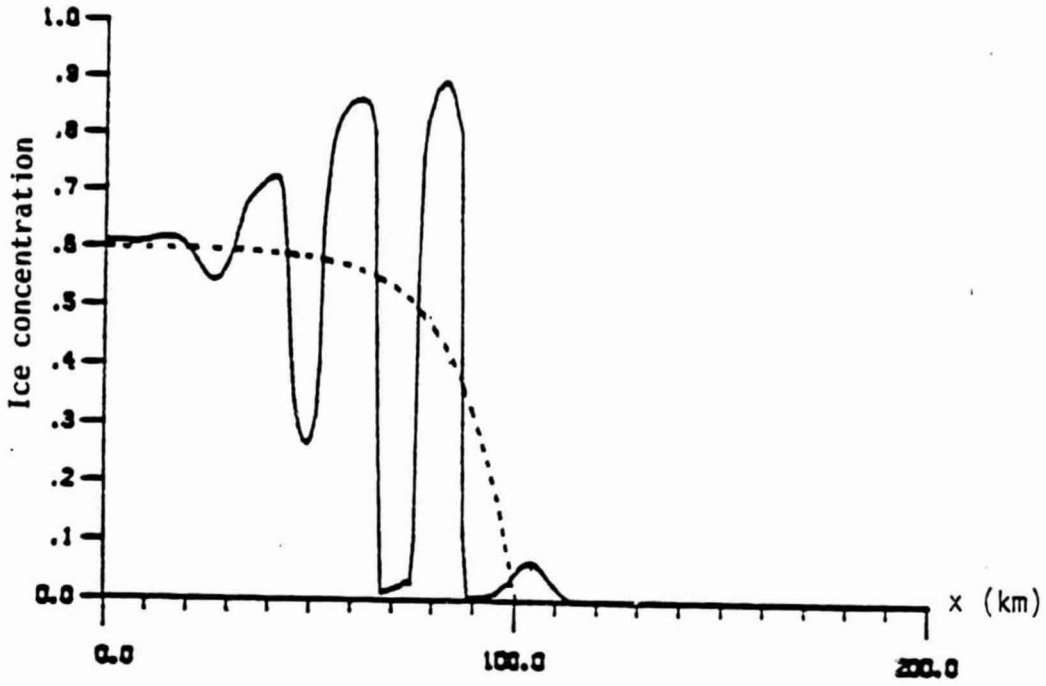

Figure 15. The ice concentration after 5 cycles of sinusoidal wind stress (period = 4 days). The dashed line refers to the initial condition. Winds vary with 10 m/s amplitude.

5. Wind Forced Eddies

In addition to barotropic and baroclinic instability processes as eddy generation sources in the MIZ, the studies of the 60-90km eddy in the Greenland Sea (Wadhams and Squire, 1983, Smith et al., 1984) can give a hint that there might be other processes. The conservation of potential vorticity can explain this cyclonic (and barotropic) vortex because it is lying on top of a deep topographic feature in the area of southerly flow. The scale of the vortex would be determined by the scale of the topographic feature, which may explain why this Greenland Sea vortex is so much different in scale compared with the other eddies seen in the Greenland MIZ.

In the above example the topography forces eddying motion in the ocean. In this section we study how external forcing like wind forcing could produce eddies at the ice edge. The satellite pictures taken from the MIZ ice cover show that the ice concentration does not follow any regular distribution along and across the ice edge direction. The disturbances in ice cover would modify the stress exerted on the ocean. Even with a constant wind field, the variation in the ice cover can generate vorticity. Since ice usually moves slower than the internal wave speed, the ocean can respond to the varying stress in such a way that up/downwelling enhancements will form.

Two cases of disturbance configurations for the ice cover are considered. In the first case the ice edge has a meandering structure and the ice concentration is constant far away from the ice edge. The second case describes disturbances in the ice concentration along the ice edge, but the ice edge itself is straight. The strong interfacial stress will make the effect of a varying ice thickness negligible compared with the first two. The two-dimensional numerical model described in section 3.1 is used where the ice thickness is taken to be constant (= 4 m). The upper layer thickness is chosen to be 25 m, so that nonlinear dynamics will be important.

5.1 Variations in the ice edge position

In order to demonstrate the dynamics it is assumed that the ice edge position takes a regular sine-wave form, figure (16), and further in the ice pack the concentration is uniform. In principle the variation can be of any kind of deviation away from a straight edge. The way these disturbances have developed is irrelevant to this problem, whether they have formed due to barotropic flow over a varying topography or different melting rates etc. The essential thing is that these features persist for several days or sufficiently long time that the ocean can develop a baroclinic response.

It is necessary that the amplitude of the ice edge "wave" is of the order of the Rossby radius of deformation so that the ocean can resolve the variation in the stress. Figure (17) provides a sketch of the oceanic response to upwelling favorable wind. The dynamics can be

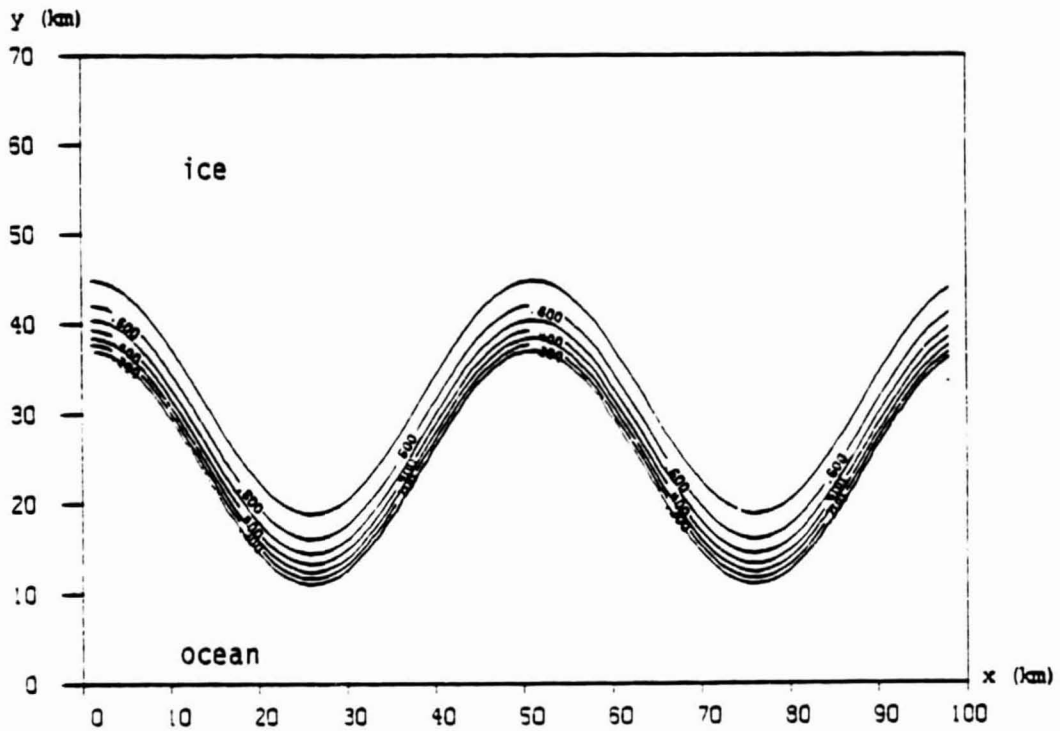

Figure 16. Wavy ice edge structure given as an initial condition for the ice concentration.

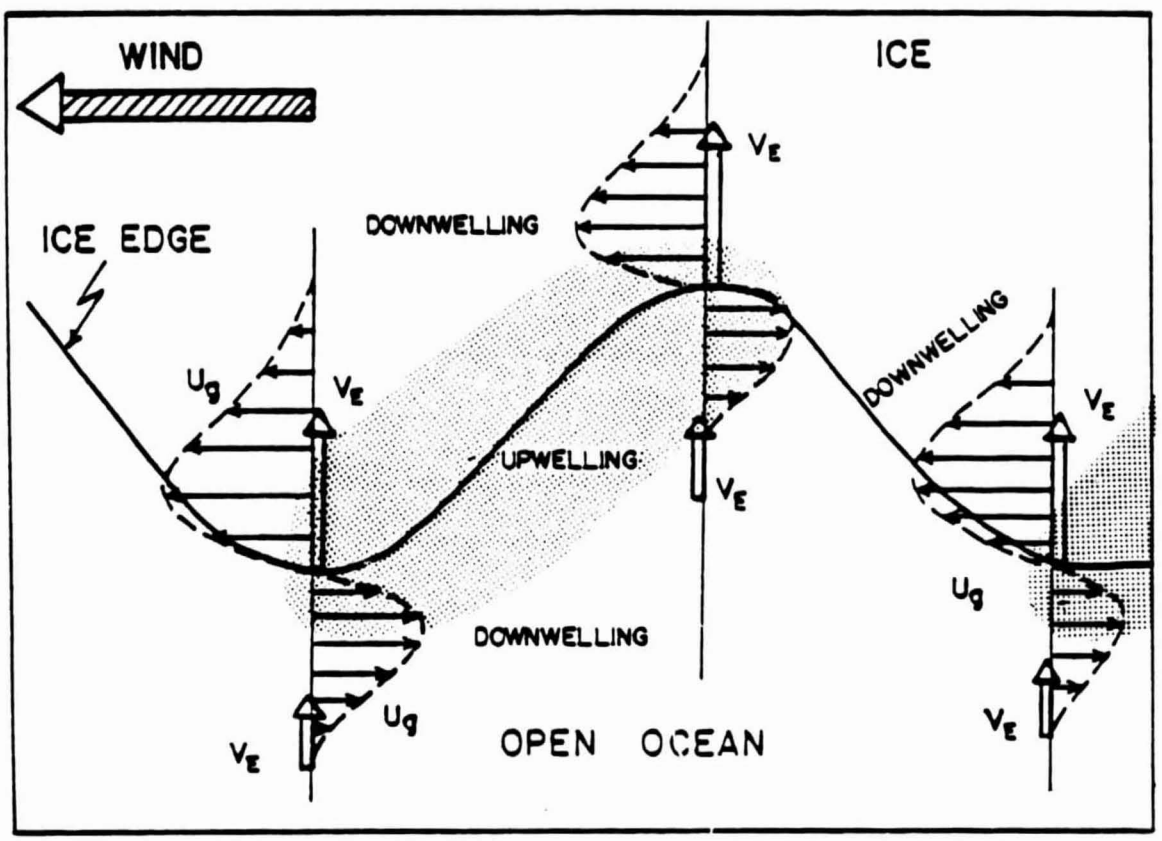

Figure 17. Schematic diagram of the dynamics when forcing is applied to the ice cover in figure 16.

explained by differential Ekman pumping: When Ekman suction is initiated at the edge, the associated upwelling jet will begin to develop. The variation in the ice edge position relative to the wind direction will lead to the nonuniformity in the oceanic jet pattern forming divergences and convergences. The up-and downwelling regions in figure (17) are imbedded in the background upwelling which exists because of the moving ice edge. The strongest upwelling signal forms on the upwind side of the ice edge "wave" (the shaded area). If the amplitude of the wave is large, this enhancement can split into two maxima, one at the crest, the other in the trough of the wave.

Given the initial condition for the ice concentration (figure 16), the model simulation was done applying upwelling favorable wind (12 ms^{-1}, 30° angle off the x-axis) for 1.5 days. Open boundary conditions were applied to the north and south, and cyclic conditions to the east and west. The ice concentration is less than 85 % everywhere for all times, which implies negligible internal ice stresses.

The resulting ice configuration and the pycnocline changes are shown in figures (18) and (19). The ice edge wave has deformed and amplified slightly, but it cannot be called unstable (figure 18). Sharp concentration gradients start to build up in the trough and in the front edge of the wave due to underlying oceanic cyclonic motion (figure 19). The maximum pycnocline change is 2.5 times higher than the background upwelling pattern. These eddies will not separate

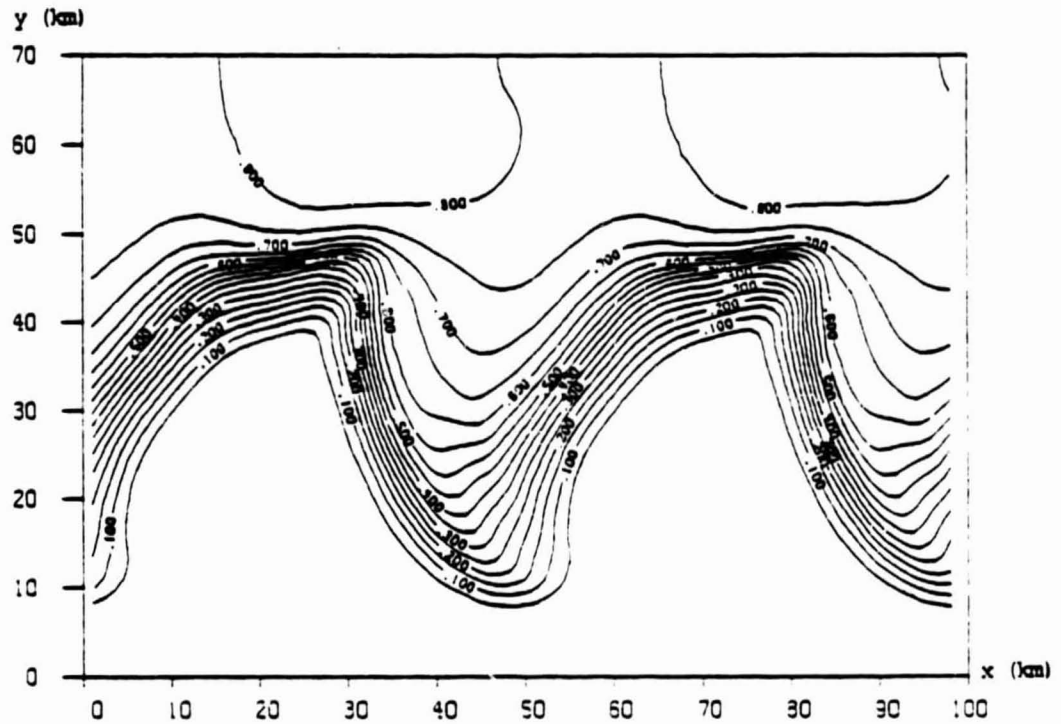

Figure 18. The ice concentration after 1.5 days of upwelling favorable winds applied on the ice cover in figure 16. Wind speed is 12 m/s.

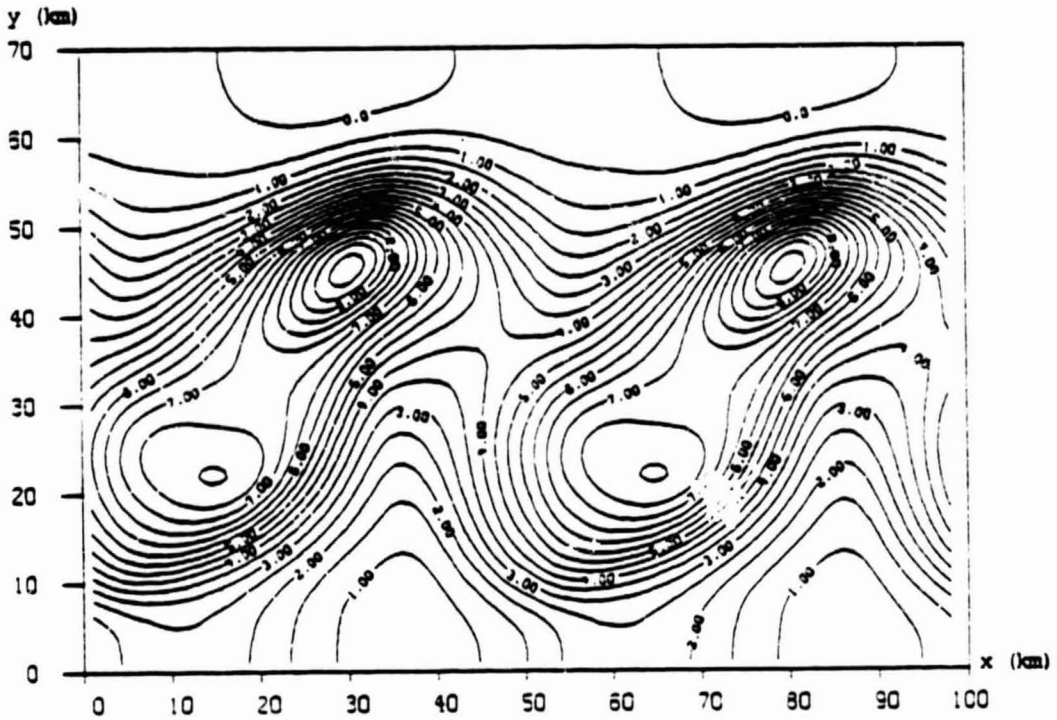

Figure 19. The pycnocline anomaly (in meters) when upwelling favorable winds are acting on the ice cover in figure 16 for 1.5 days.

from the ice edge, they will stay connected to the ice edge disturbance that supports their existence and move with the same speed as the ice. Eventually these upwelling enhancements will surface, but the simulation was not carried that far. The pycnocline tilt, higher in the southern part of the region, is needed to compensate the velocity in the x-direction induced by the moving ice.

5.2 Varying ice concentration

In this class of disturbances there is a straight ice edge but the ice concentration varies along the ice edge direction. Again the initial distribution of the ice concentration in the model simulation has been chosen to have a simple sinusoidal form (figure 20), the wave length of the variation being 50 km. The concentration variation further out does not play an important role in the dynamics.

Figure (21) shows the principles of the oceanic response to upwelling favorable wind. The Ekman transports underneath the ice are higher in areas where there are high ice concentrations (differential Ekman pumping). This implies that the pycnocline changes are larger in high concentration areas than in low concentration areas. Furthermore, the geostrophic currents associated with these pycnocline changes vary accordingly, which produces upwelling enhancements behind the concentration maxima as shown in figure (21) with shading.

Taking the initial conditions of figure (20) and applying the

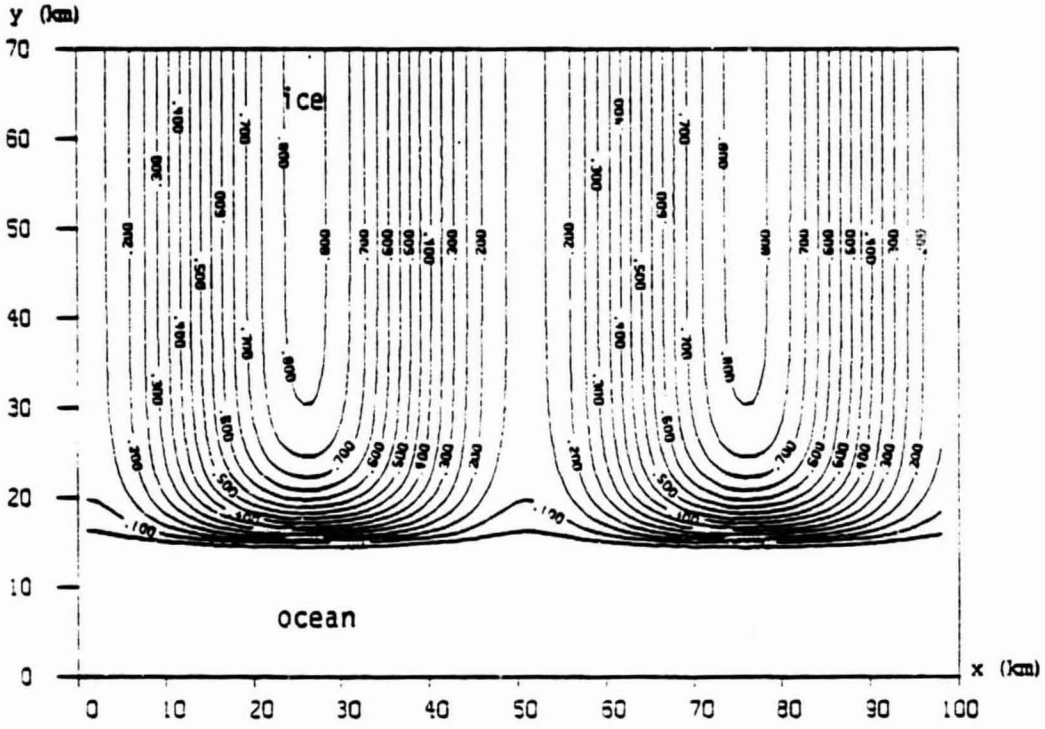

Figure 20. The initial condition for the ice concentration with variation along the (straight) ice edge.

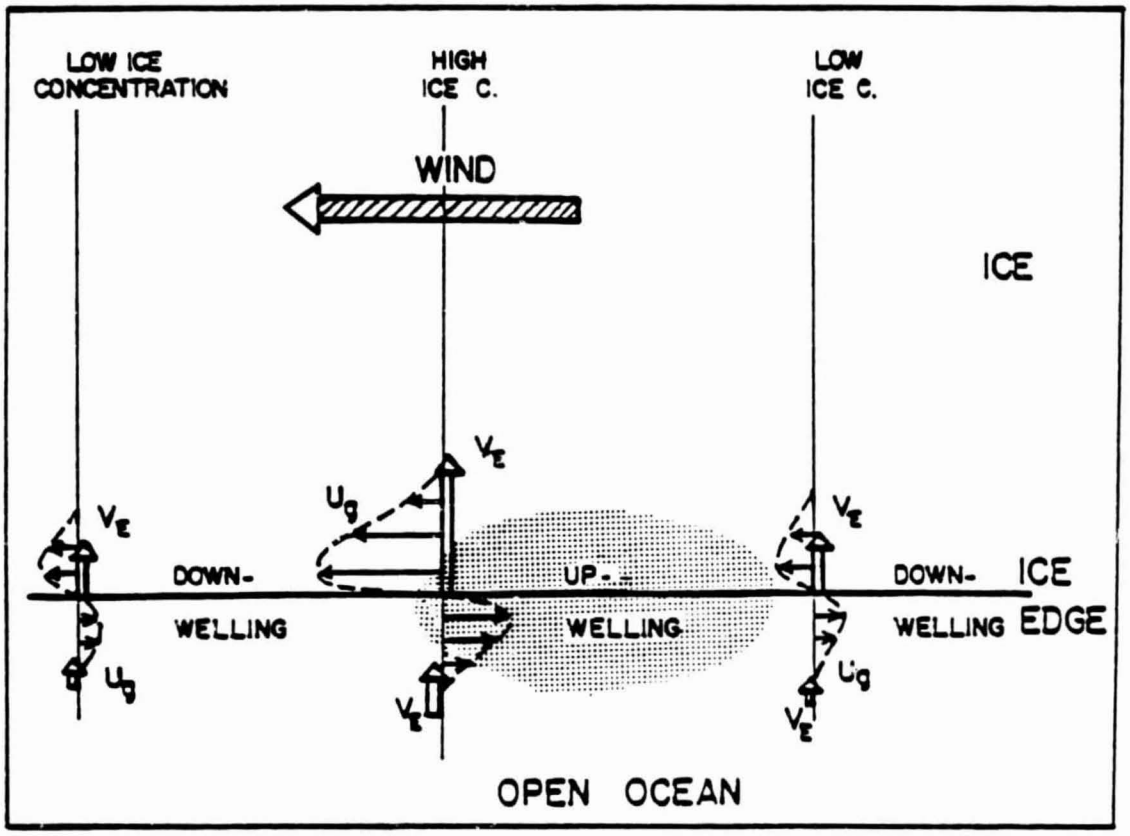

Figure 21. Schematic diagram of the forced dynamics in the ocean coupled to the ice cover in figure 20.

same wind field as in the earlier case (12 ms^{-1} inclined 30° from the x-axis) the results after 1.5 days are shown in figures (22) and (23). As seen there are negligible changes in the ice configuration. The variation in the 10% concentration line has gained some more amplitude, but the ice edge itself is nearly straight. The oceanic structure underneath (figure 23) does not manifest itself clearly in the ice cover. The pycnocline enhancement is nearly twice in amplitude than the average upwelling signal. In this as in the earlier case the enhancement is strictly tied to the ice concentration distribution and the "eddy" moves with the speed of the ice. In the front edge of the disturbance the upwelling enhancement is destroyed and behind it created again and amplified (figure 23). Furthermore, the ice is essentially in a state of free drift (as in the earlier case), because at low ice concentrations (less than 85%) the internal ice stresses are vanishingly small.

5.3 Eddy shedding

In the one-dimensional case the time varying forcing produced a distinctive pattern of up- and downwelling signals (and ice bands). The nonlinear advection terms redistributed the vorticity so that the pycnocline changes (vortex tube stretching) were preserved in wind reversals. In the following we study a possibility of shedding eddies at the ice edge under similar conditions.

For the ice cover variation in section 5.2, a simulation of

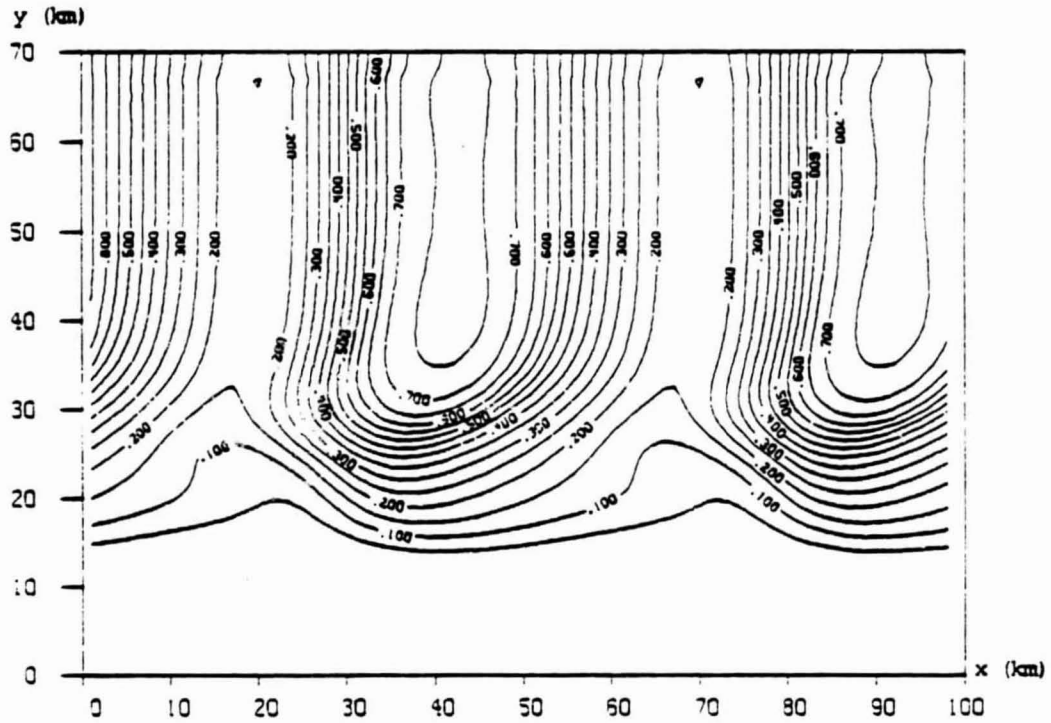

Figure 22. The ice concentration after 1.5 days of upwelling favorable wind of 12 m/s exerted on the ice cover in figure 20.

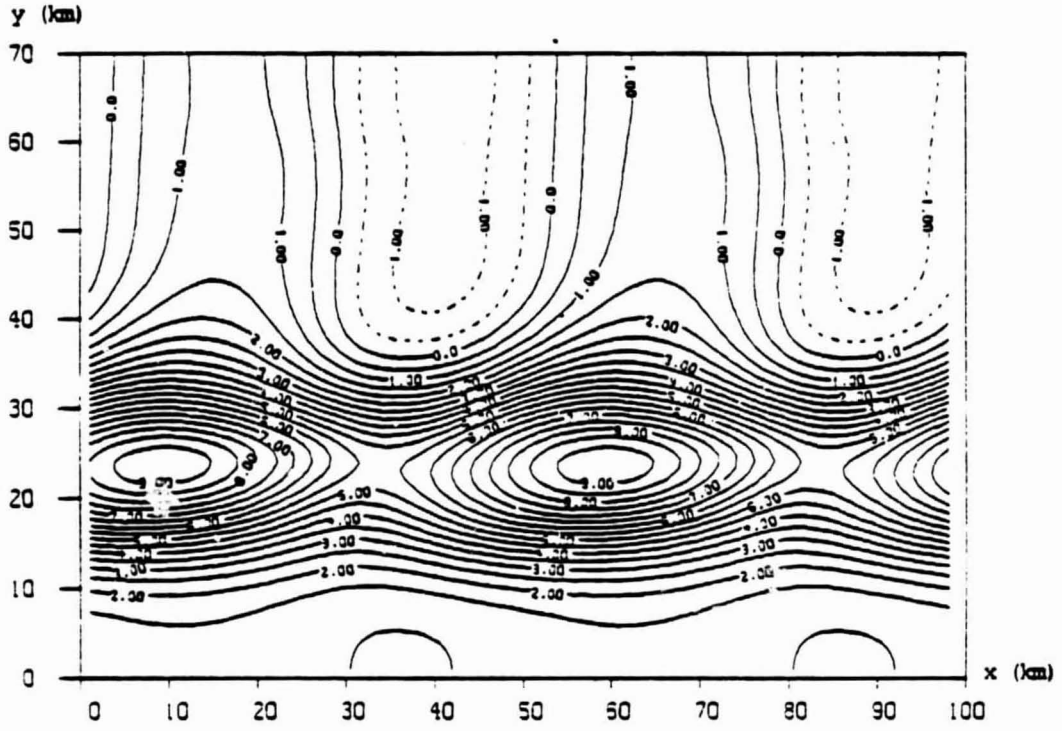

Figure 23. The pycnocline anomaly (in meters) after 1.5 days of upwelling underneath the ice cover in figure 22.

passing of a cyclone was done. Starting from the conditions at 1.5 days, the winds were turned gradually off in 3 hours and increased back in 3 hours but to the opposite direction. The resulting ice configuration at 3.0 days is shown in figure (24). Now the ice edge looks like a breaking wave, with a small amount of ice outside the very sharp ice concentration gradient. Underneath the wave like feature in the ice cover the ocean response is in the form of a cyclonic eddy that previously was a mere enhancement in the upwelling zone and hidden underneath the main ice pack (figure 25).

The dynamical reason for this shedding of eddies is the nonlinear interaction that appears in the vorticity equation (3.3.12) as advection of the wave pattern with the Ekman velocity. When the winds reverse, the Ekman transports also change to the opposite direction, from northward to southward advecting the upwelling enhancements out to the open ocean. In this way the temporally varying Ekman transport redistributes vorticity which is supplied by the winds acting on a nonuniform ice cover, i.e. the variation in the ice cover acts like bottom topography. This eddy formation resembles the topographically generated eddies due to temporally varying mean flow discussed by Huppert and Bryan (1976).

If the model were linear, the generated upwelling enhancements would be destroyed in wind reversals. In this nonlinear formulation the cyclonic eddies are shed to the open water in wind reversals, but the anticyclonic ones would be advected underneath the ice.

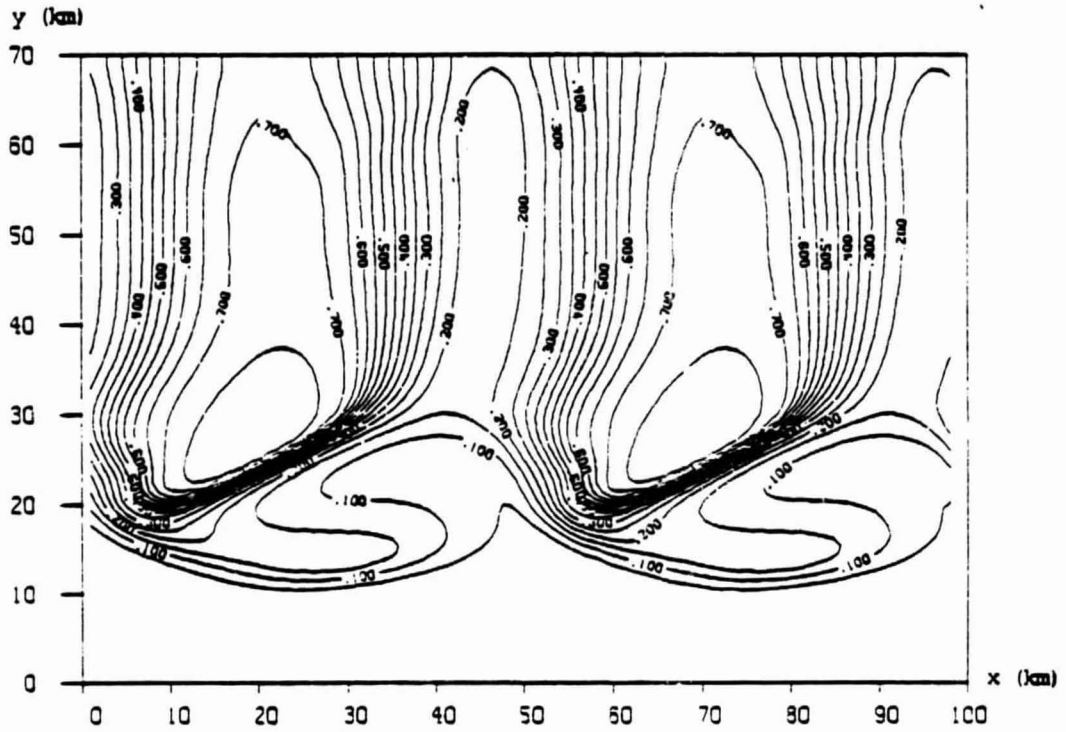

Figure 24. The ice concentration with strong ice edge meanders after 1.5 days of downwelling favorable winds (12 m/s). The initial conditions are as in figures 22 and 23.

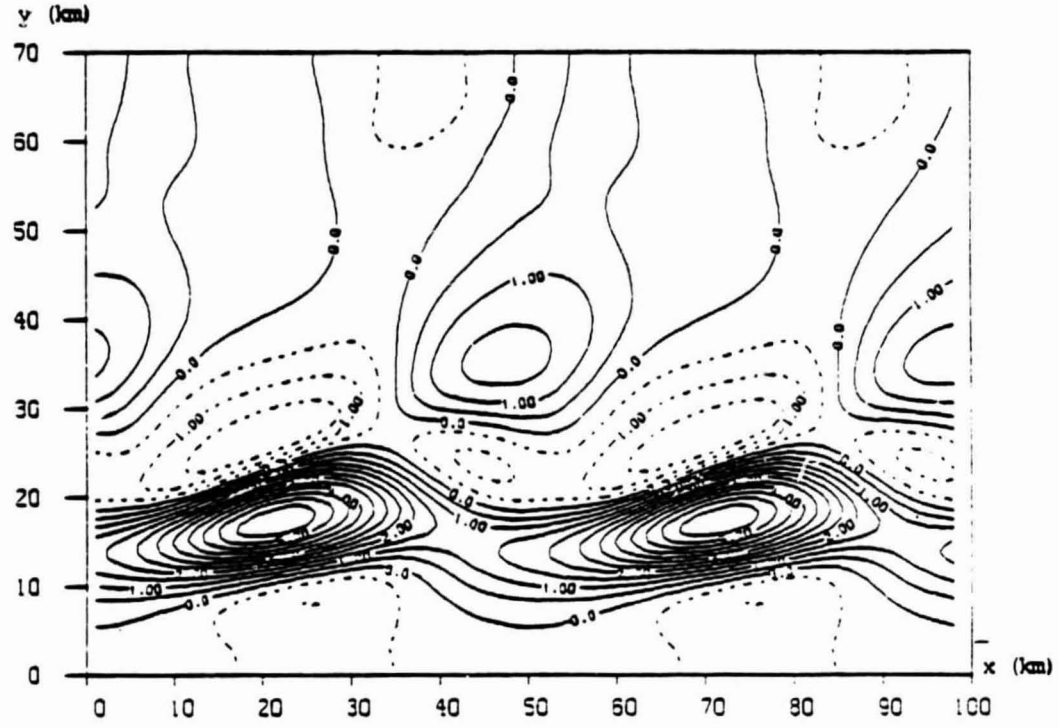

Figure 25. The pycnocline anomaly (in meters) showing the eddy shedding after reversing the winds to downwelling favorable for 1.5 days. Initial conditions are as in figure 22 and 23.

6. Discussion and conclusions

The aim of this study is to model the mesoscale dynamics in the marginal ice zones by means of a two-dimensional coupled ice-ocean model. The major focus is to study the baroclinic response of the ocean to forcing by the winds and moving ice on time scales of a few days. The sea-ice model is coupled to the reduced gravity ocean model through a stress on the ice-ocean interface.

In some of the earlier studies the internal ice stress was crucial to the dynamics due to the chosen plastic-viscous stress law of ice. In this work the internal stresses were formulated on the basis of the Reiner-Rivlin theory, which means that sea ice is a viscous medium where the viscosity coefficients depend on the strain rate invariants and external parameters like the concentration and and thickness of the ice. For typical MIZ ice concentrations the stresses are negligible, and only when the ice converges strongly they can be effective. The main dynamical balance in the ice is between the water-ice stress and the wind stress, i.e. free drift.

In the reduced gravity ocean model two cases were considered, a linear case where the upper layer is thick and a nonlinear one where the upper layer is thin. The latter corresponds to typical conditions in the late summer, early fall in the Greenland Sea. In the

model the drag coefficients are chosen so that the air-ice stress is three times bigger than the air-ocean stress, and also so that the ice-ocean coupling is strong. With this choice of parameters winds parallel to the ice edge, ice on the right, can produce upwelling, because the Ekman transport is much greater under the ice than in the open ocean. In the nonlinear case an oceanic front starts to develop together with a strong convergence of the ice edge during three to four days of upwelling favorable wind. With a thick upper layer the upwelling signal is nearly symmetric and also the ice is strongly diverging at the edge. The frontal structure is clearly seen in the summertime observations from the Greenland Sea.

The barotropic stability analysis was carried out for the computed up- and downwelling jets in the thin upper layer case. The most unstable wavelength is 20-30 km. For moderate ice concentration gradient at the edge, the growth rates of the upwelling jet are very slow. It can be considered nearly stable because e-folding time is of order of several tens of days, only in the case of a step-like ice edge can there be high growth rates. The upwelling jet is stabilized due to the divergence. In the downwelling this term is negligible and the jet appears to be extremely unstable. In general, the growth rates depend strongly on the strength and direction of the wind, because the wind together with the ice concentration gradient determine the up/downwelling jet profile.

The simple one-dimensional upwelling simulation was extended to include temporally varying forcing, which was chosen to vary sinusoidally with a 4 day period. The setup is designed to resemble cyclone passings perpendicular to the ice edge. The linear model is not of great interest, since the upwelling signal only grows and decays symmetrically with changing wind direction. In the nonlinear case the formed up-and downwelling responses do not vanish in the successive wind reversals. The advection of wave patterns due to Ekman velocities shifts the up-(or down)welling signal away from the area where the reversed winds could destroy it. The variation of the pycnocline is the originating force for the ice bands: the varying upper layer thickness leads to convergences and divergences in the Ekman velocities which are then reflected in the ice velocities due to the strong ice-water coupling. Also after 1 1/2 cycles the ice cover variation starts to enhance the pycnocline structure, and the ice cover actually has taken a banded structure near the ice edge.

The width of the produced bands is about two Rossby radii of deformation which is the smallest scale for the pycnocline variation at the ice edge. There must be at least one wind reversal to produce one band. This theory can well account for the Bering Sea ice bands that are seen mostly in wintertime when the ice is lying on top of a strongly stratified ocean. Furthermore, in the Bering Sea the most frequent track of cyclones is from west to east or slightly curving northeast, which is nearly perpendicular to the ice edge.

It is shown that not only the existence of the ice edge but also a variation of the ice cover in the ice edge direction can lead to pycnocline changes when the system is forced externally. The varying ice cover together with wind forcing acts like small storm systems passing, but because the ice moves very slowly the baroclinic response of the ocean is possible. The way the variation in the ice cover has developed is not of importance, and it is assumed that its evolution time is far greater than the baroclinic time scale. For instance, barotropic mean flow over topographic disturbances can be reflected in the ice edge disturbances or in the ice concentrations. If the barotropic mean flow is slow, there is not much coupling between barotropic and baroclinic components due to ice.

The scales of the ice cover variability determine the oceanic scales, the smallest scale being the Rossby radius of deformation. If the cross-ice edge and along the ice edge scales are about the same order the oceanic response to upwelling favorable winds looks like a cyclonic eddy. Typically, the scales of these forced eddies can be from 2 to 10 times the Rossby radius of deformation. This is the same scale range where the eddies generated through instability processes would belong. The eddy-like features are more pronounced if the supporting ice cover variation is in the ice edge itself than in the ice concentration (the ice edge being straight). The nonuniformity of the ice cover generates vorticity which is transferred through the differential Ekman pumping into the eddy motion in the

ocean. The forced eddies move with the speed of the ice, and are always attached to the ice disturbance that supports them when there are no changes in the forcing.

It is shown that ice cover disturbances can shed eddies to the open ocean with temporally varying wind fields. This is dynamically similar to forming ice bands; the nonlinear advection of the wave pattern due to the Ekman velocity shifts the upwelling enhancement to the open ocean when winds reverse. The formed eddies force the ice edge to meander strongly. If anticyclonic eddies were produced, they would disappear underneath the ice cover leaving no trace of their existence around the ice edge. This eddy formation hypothesis supports the fact that cyclonic eddies are more abundant in the satellite pictures which can only show the eddies in the open ocean.

There is a strong resemblance between varying ice cover and bottom topography, because ice cover also couples the barotropic and baroclinic motion, even though in this model only the baroclinic ocean is considered. In the case that the ice-water stress is negligible, there can be decoupling. Barotropic flow (externally or locally driven) forces the ice to move which in turn forces up/downwelling in the baroclinic part at the ice edge. If the barotropic flow is externally driven then up/downwelling can occur without winds. The effect of topography and the feedback between barotropic and baroclinic flows and the moving ice are needed for the full dynamical description of MIZ.

Appendix

Assuming that the stress depends on the strain rate only, the stress tensor (of rank two) may in general be written in the form

$$\underset{\sim}{\sigma} = g(\dot{\underset{\sim}{\varepsilon}}).$$

The principle of generalized dimensions requires that all terms on the right-hand side are sums of mixed tensors of rank two only, possibly multiplied by scalars, and of inner products of such tensors which again reduce to tensors of rank two. The stress-strain relation may be written

$$\underset{\sim}{\sigma} = \sum_{n=1}^{\infty} f_n(\theta_1,\theta_2,\theta_3)\dot{\underset{\sim}{\varepsilon}}^n , \tag{1}$$

or

$$\underset{\sim}{\sigma} = f_0(\theta_1,\theta_2,\theta_3)\underset{\sim}{1} + f_1(\theta_1,\theta_2,\theta_3)\dot{\underset{\sim}{\varepsilon}} + f_2(\theta_1,\theta_2,\theta_3)\dot{\underset{\sim}{\varepsilon}}^2 \tag{2}$$

$$+ f_3(\theta_1,\theta_2,\theta_3)\dot{\underset{\sim}{\varepsilon}}^3 + \ldots$$

where $\theta_1,\theta_2,\theta_3$ are the three strain rate invariants, viz.,

$$\theta_1 = \mathrm{tr}\dot{\underset{\sim}{\varepsilon}} ,$$

$$\theta_2 = (\theta_1^2 - \mathrm{tr}\dot{\underset{\sim}{\varepsilon}}^2)/2 ,$$

$$\theta_3 = \det\dot{\underset{\sim}{\varepsilon}} ,$$

where tr stands for trace and det for determinant.

Applying the Cayley-Hamilton theorem, all terms of order higher

than $\underset{\sim}{\dot{\varepsilon}}^2$ reduces to order $\underset{\sim}{1}$, $\underset{\sim}{\dot{\varepsilon}}$ and $\underset{\sim}{\dot{\varepsilon}}^2$ terms, i.e.

$$\underset{\sim}{\dot{\varepsilon}}^3 = \theta_1 \underset{\sim}{\dot{\varepsilon}}^2 - \theta_2 \underset{\sim}{\dot{\varepsilon}} + \theta_3 \underset{\sim}{1}$$

Thus, (1) may be written

$$\underset{\sim}{\sigma} = \phi_1(\theta_1,\theta_2,\theta_3)\underset{\sim}{1} + \phi_1(\theta_1,\theta_2,\theta_3)\underset{\sim}{\dot{\varepsilon}} + \phi_2(\theta_1,\theta_2,\theta_3)\underset{\sim}{\dot{\varepsilon}}^2$$

In two dimensions $\theta_2 = \theta_3$, and the Cayley-Hamilton theorem reduces to

$$\underset{\sim}{\dot{\varepsilon}}^2 - \theta_1 \underset{\sim}{\dot{\varepsilon}} + \theta_2 \underset{\sim}{1} = 0$$

because

$$\begin{vmatrix} \dot{\varepsilon}_1-\lambda & 0 \\ 0 & \dot{\varepsilon}_2-\lambda \end{vmatrix} = \dot{\varepsilon}_1\dot{\varepsilon}_2 - (\dot{\varepsilon}_1+\dot{\varepsilon}_2)\lambda + \lambda^2 = 0$$

Thus the polynomial expansion (1) reduces to

$$\underset{\sim}{\sigma} = \phi_0'(\theta_1,\theta_2)\underset{\sim}{1} + \phi_1'(\theta_1,\theta_2)\underset{\sim}{\dot{\varepsilon}} .$$

C-2

References

Alexander, V., 1980: Interrelationships between the seasonal sea ice and biological regimes, Cold Reg. Sci. Tech., 2, 157-178.

_____, and H. J. Niebauer, 1981: Oceanography of the eastern Bering Sea ice-edge zone in spring, Limnol. Oceanogr., 26, 1111-1125.

Astarita, G., and G. Marrucci, 1974: Principles of non-Newtonian fluid mechanics, McGraw-Hill, 289 pp.

Bauer, J., and S. Martin, 1980: Field observations of the Bering Sea ice edge properties during March 1979, Mon. Weather Rev., 108, 2045-2056.

Buckley, J. R., T. Gammelsrod, J. A. Johannessen, O. M. Johannessen and L. P. Roed, 1979: Upwelling: Oceanic structure at the edge of the Arctic ice pack in winter, Science, 203, 165-167.

Campbell, J. W., 1965: The wind-driven circulation of ice and water in polar ocean, J. Geophys. Res., 70, 3279-3301.

Clarke, A. J., 1978: On wind-driven quasi-geostrophic water movement at fast ice edges, Deep-Sea Res., 25, 41-51.

Coachman, L. and K. Aagaard, 1974: Dynamical Oceanography of Arctic and Subarctic Seas, in Marine Geology and Oceanography of the Arctic Sea, Springer-Verlag, N.Y.

Colony, R., and R. S. Pritchard, 1975: Integration of elastic-plastic constitutive laws, AIDJEX Bulletin, 30, 55-81.

Coon, M. D., 1974: Mechanical behavior of compacted Arctic ice floes, J. Petrol. Tech., 26, 446-470.

_____, 1980: A review of AIDJEX modelling, in Sea Ice Processes and Models (R.S. Pritchard, ed.) Univ. of Washington Press, Seattle.

_____, G. A. Maykut, R. S. Pritchard and D. A. Rothrock, 1974: Modelling the pack ice as an elastic-plastic material, AIDJEX Bulletin, 24, 1-105.

Doronin, Yu. P., 1970: Methods of computation of ice compaction and drift, Trudy AANII, 291, Leningrad.

Gammelsrod, T., M. Mork and L. P. Roed, 1975: Upwelling possibilities at an ice-edge, homogeneous model, Mar. Sci. Comm., 1, 115-145.

Glen, J. W., 1958: The flow law of ice: a discussion of the assumptions made in glacier theory, their experimental foundations and consequences, IUGG/AIHS Symposium de Chamonix, 16-24 Sept. 1958, 254-265.

_____, 1970: Thoughts on a viscous model for sea ice, AIDJEX Bulletin, 2, 18-27.

Gorshkov, S. G. (ed.), 1983: World Ocean Atlas, volume 3, Arctic Ocean, Pergamon Press, Oxford.

Hart, J. E., and P. D. Killworth, 1976: On open ocean baroclinic instability in the Arctic, Deep-Sea Res., 23, 637-645.

Hibler, W. D., III, 1977: A viscous sea ice law as a stochastic average of plasticity, J. Geophys. Res., 82, 3932-3938.

_____, 1979: A Dynamic-Thermodynamic sea ice model, J. Phys. Oceanogr., 9, 815-846.

_____, and W. B. Tucker, III, 1979: Some results from a linear-viscous model of the Arctic ice cover, J. Glaciol., 22, 293-304.

_____, and J. E. Walsh, 1982: On modeling seasonal and interannual fluctuations of Arctic sea ice, J. Phys. Oceanogr., 12, 1514-1523.

Hunter, S. C., 1976: Mechanics of continuous media, Horwood Ltd., 567 p.

Huppert, H. E., and K. Bryan, 1976: Topographically generated eddies, Deep-Sea Res., 23, 655-679.

Johannessen, J. A., O. M. Johannessen, E. Svendsen, B. Farrelly, H. Royset, A. Holm, A. Revheim, B. Biskopshavn, S. Myking and F. C. Svendsen, 1980: A CTD-data report from the NORSEX marginal ice zone program north of Svalbard in September-October 1979, Univ. of Bergen, Bergen, Norway, 1980.

Johannessen, O. M., J. A. Johannessen, J. Morison, B. A. Farrelly and E.A.S. Svendsen, 1983: The mesoscale oceanographic conditions in the marginal ice zone north of Svalbard in early fall 1979, J. Geophys. Res., 88, 2755-2769.

Macklin, S. A., 1983: Wind Drag Coefficient Over First-Year Sea Ice in the Bering Sea, J. Geophys. Res., 88, 2845-2852.

McPhee, M. G., 1980: An analysis of pack ice drift in Summer, in Sea Ice Processes and Models, (ed. R. S. Pritchard), pp. 62-75. University of Washington Press, Seattle.

_____, 1982: Sea ice drag laws and simple boundary layer concepts, including application to rapid melting, CRREL Report 82-4.

Mork, M., 1983: Private communication.

Muench, R. D., and R. L. Charnell, 1977: Observations of medium scale features along the seasonal ice edge in the Bering Sea, J. Phys. Oceanogr., 7, 602-606.

_____, P. H. LeBlond and L. E. Hachmeister, 1983: On some possible interactions between internal waves and sea ice in the marginal ice zone, J. Geophys. Res., 88, 2819-2826.

Niebauer, H. J., 1982: Wind and melt driven circulation in a marginal ice edge frontal system: a numerical model, Cont. Shelf Res., 1, 49-98.

Nikolayev, S. G., 1973: Experiment in organizing oceanographic investigations of the ice-edge zone of the Chuckhi Sea, Problemy Arktikii Antarktikii, 42, 31-36.

Pease, C. H., S. A. Salo and J. E. Overland, 1983: Drag measurements for first-year sea ice over a shallow sea, J. Geophys. Res., 88, 2853-2862.

Phillips, N. A., 1954: Energy transformations and meridional circulations associated with simple baroclinic waves in a two-level, quasi-geostrophic model, Tellus, 6, 273-280.

Pritchard, R. S., 1975: An elastic-plastic constitutive law for sea ice, J. Appl. Mech., 42 E, 379-384.

_____, 1980: A simulation of nearshore winter ice dynamics in the Beaufort Sea, in Sea Ice Processes and Models (R.S. Pritchard ed.) Univ. of Washington Press, Seattle.

_____, and R. Reimer, 1978: Mathematical characteristics of a plastic model of sea ice dynamics, AIDJEX Bulletin, 40, 109-151.

Reiner, M., 1945: A mathematical theory of dilatancy, Am. J. Math., 67, 350-362.

Rivlin, R. S., 1948: The hydrodynamics of non-Newtonian fluids, I, Proc. Roy. Soc. (London), A193, 260-281.

Rivlin, R. S., 1955: Further remarks on stress-deformation relations for isotropic material, J. Rat. Mech. Anal., 4, 681-702.

Roed, L. P., 1983: Sensitivity studies with a coupled ice-ocean model of the marginal ice zone, J. Geophys. Res., 88, 6039-6042.

Roed, L. P., and J. J. O'Brien, 1981: Geostrophic adjustment in highly dispersive media, An application to the marginal ice zone, Geophys. Astrophys. Fluid Dynamics, 18, 263-278.

_____, and _____, 1982: A coupled ice-ocean model of upwelling in the marginal ice zone, J. Geophys. Res., 88,2863-2872.

Rothrock, D. A., 1975: The energetics of the plastic deformation of pack ice by ridging, J. Geophys. Res., 80, 4514-4519.

_____, 1979: Modeling sea-ice features and processes, J. Glaciol., 24, 359-374.

Smedstad, O. M., and L. P. Roed, 1984: A coupled ice-ocean model of ice break-up and banding in the marginal ice zone, to appear in J. Geophys. Res.

Smith, D. C., J. H. Morison, J. A. Johannessen and N. Untersteiner, 1984: Topographic generation of an eddy at the edge of the East Greenland current, J. Geophys. Res., 89, 8205-8208.

Smith, R. B., 1983: A note on the constitutive law for sea ice, J. Glaciol., 29, 191-195.

Swift, J. H., and K. Aagaard, 1981: Seasonal transitions and water mass formation in the Iceland and Greenland Seas, Deep-Sea Res., 28A, 1107-1129.

The Polar Group, 1980: Polar atmosphere-ice-ocean processes: A review of polar problems in climate research, Rev. Geophys. Space Phys., 18, 525-543.

Vinje, T. E., 1977: Sea ice studies in the Spitsbergen-Greenland area, Landsat Rep. E77-10206, U. S. Dept. of Commerce, Natl. Tech. Inf. Ser., Springfield, Va.

Wadhams, P., 1981: The ice cover in the Greenland and Norwegian Seas, Rev. of Geophys. Space Phys., 19, 345-393.

_____, 1983: A mechanism for the formation of ice edge bands, J. Geophys. Res., 88, 2813-2818.

Walter, B. A., J. E. Overland and R. O. Gilmer, 1984: Air-Ice Drag Coefficients for First-Year Sea Ice Derived From Aircraft Measurements, J. Geophys. Res., 89, 3550-3560.